63-4-2

Doc. # 757 A
Copy # 19

FINAL REPORT

MILLIMETER PROGRAM

CONTRACT NO. AF33(616) - 7414

JUNE 1, 1960 - APRIL 30, 1963

PREPARED FOR:

UNITED STATES AIR FORCE
AFSC AERONAUTICAL SYSTEMS DIVISION
WRIGHT PATTERSON AIR FORCE BASE, OHIO

PREPARED BY:

EWEN KNIGHT CORPORATION
EAST NATICK, MASSACHUSETTS

TABLE OF CONTENTS

1.0 28 FOOT PRECISION PARABOLIC ANTENNA SYSTEM

1.1 Antenna Complex

The antenna complex is one of the most important single items of this program. It includes the reflector its back-up structure, the spar support and the horn ring. The following sections summarize the efforts expended on the design and implementation of the antenna during this initial period.

1.1.1 Antenna Design Considerations

Design considerations of the antenna include the: (1) existing pedestal, (2) size and weight, and (3) surface accuracy. Fundamental to the selection of a millimeter antenna is the existing pedestal at Ewen Knight's Needham Test Facility. The restriction it presents is the pointing accuracy of the mount. This, among other things, is a function of the mechanical stiffness of the pedestal and the positioning capability. The pedestal with its present antenna, was designed to an accuracy of one (1) minute of arc; therefore, any new antenna must be compatible with the pedestal and previous antenna configuration so that its pointing accuracy does not deteriorate from the intended overall accuracy. The similarity in configuration requires the shape factor of the old and new antennas to be within 10 to 15 percent of each other.

The maximum size of the antenna is determined by the size of the radome that can be used on the existing building and still retain its stability during high winds up to 100 mph. Structural load calculations conclude that this is about 52 feet in diameter. The weight of the antenna is rather critical in that it must not affect the pedestal with an overload which might detract from the pointing accuracy. The antenna weight should not exceed 10 to 15 percent of the antenna now at the Test Facility or a maximum of 2250 lbs.

A spin cast type of antenna cannot be used on the existing pedestal because of its gross weight of 7500 lbs. The pedestal could not support this, and the servos could not drive it since this is more than 3.5 times the existing mass. Further, this antenna is too deep and would not fit in the existing radome.

The surface tolerance of the antenna cannot exceed 20 mils rms and 40 mil peak-to-peak from the ideal curve when facing either the horizon or zenith under static conditions in order to insure efficient operation up to 75 Kmc.

1.1.2 Spar Support Structure

The spars project forward from the rim of the reflector and are attached to the horn ring to which the feed system and the first stages of amplification are mounted. The rigidity of this structure is of utmost importance because of the position requirements of the feed horn. The design criteria for the spars were treated by considering mechanical static deflections due to the spars' own weight, and due to a maximum 50 pound package of RF components and receiver electronics. Two cases were treated, Case I, when the antenna is facing the horizon, and Case II, when facing the zenith. In addition, consideration was given to the effects of temperature over the operating temperature range (50° to 140°F.) Two cases were treated. Case I, the growth of the antenna over the temperature range and Case II, the growth of the spars due to the change in temperature.

Various methods for keeping the feed horn in the focal plane were studied and, are listed below.

1. Pressurizing the entire spars which result in physical stretching of the spars as in a tension spring.
2. Use of a low pressure hydraulic system with a hydraulic jack in each spar near the horn ring.
3. Heating each spar with an internal heater.
4. A mechanical carriage with two degrees of freedom.

Summary of Design Criteria

The motion along the boresight axis using spars that extend one foot beyond the focal plane with a 12 inch horn ring are:

A. Mechanical Statis Deflections

Case I Antenna Facing the Horizon

Translation Component Along Boresight Axis	Size of the Spar	Size of Horn Ring
-0.028 ins.	4" O.D. x .125"t	12" I.D.
-0.010 "	6" O. D. x .312"t	" "
-0.007 "	8" O.D. x .188"t	" "
-0.003 "	11" O.D. x .188"t	" "

t denotes wall thickness

Case II, Antenna Facing the Zenith

Translation Component Along Boresight Axis	Size of the Spar	Size of Horn Ring
-0.053 ins.	4" O.D. x .125"t	12" I.D.
-0.052 "	6.5" O.D. x .312"t	" "
-0.030 "	8" O.D. x .188"t	" "
-0.016 "	11" O.D. x .188"t	" "

B. Effects of temperature.

Change in configuration due to $\Delta T = 90^{\circ}F$.

1. Spar change in length = + .096 inches

2. Antenna change in length = + .044 inches

Total change along boresight axis = + .140 inches.

Summary Cases I and II

Total Motion Due to Static Deflection and Temperature

Size of Spar	Total Deflection Case I	Total Deflection Case II
4" O.D.	+ .112"	+ .187"
6.5" O.D.	+ .130"	+ .088"
8" O.D.	+ .133"	+ .110"
11" O.D.	+ .137"	+ .124"

From the summary data, it is reasonable to conclude that aluminum spars with the least diameter present the least defocusing along the boresight axis due to the spars' own static weight plus a 50 pound R.F. package located near the horn ring. It should be noted that the temperature effect on the spars and the reflector are somewhat self compensating due to the all aluminum structure. The .312" wall spar will heat up slower than thinner wall spars due to increased temperature and therefore is more effective in stabilizing the spare structure. In addition, the smaller spar presents the least aperture blockage to the incoming signal. The 6.50" O.D. x .312" wall thickness aluminum spars were chosen to optimize all the design criteria. It is planned to insulate the spars to reduce effects of temperature.

1.1.3 Approach Selected

Since the antenna complex is a key item in this program, Ewen Knight expended considerable care and effort in evaluating the capabilities of various vendors who proposed to do the fabrication.

Table 1 summarizes this information.

TABLE 1

SUMMARY

PROPOSED MILLIMETER ANTENNAS

Antenna Contractor	Antenna Systems, Inc., Hingham, Massachusetts	Philco W.D. Labs, Palo Alto, California	D.S. Kennedy Cohasset, Massachusetts	T.R.G., Inc. Somerville, Massachusetts	Goodyear Aircraft Corp., Akron, Ohio
Size	30 feet	28 feet	28 feet	28 feet	28 feet
Delivery	90 days	5 months	3 months	4 months	40 weeks
Fixed Price	$16,500	$64,100	$12,950	$79,951	$94,087
Conforms to E.K. Spec.	Marginal	Yes	Yes	Yes, possible weight exception	Incomplete
Remarks	Price includes installation; measuring technique is crude.	Requires E.K. provide shelter from sun and wind during assembly.	Includes installation.	Price does not include complete installation.	Price does not include counterweight, structural tie to pedestal, nor installation changes.

Selected Component Approach

The approach selected was based upon choosing a somewhat stiffer antenna than the existing one, having a composite surface that is within .020" rms. of the perfect paraboloid.

Based upon these considerations and confidence in vendors, a purchase order for an antenna, spar and counterweight configuration from D.S. Kennedy, Cohasset, Massachusetts was released in accordance with our specifications.

To substantiate the confidence in the proposed antenna, a brief discussion of the deficiencies in the antenna, presently at the Ewen Knight Test Facility, and the techniques used in manufacturing and measuring the proposed antenna are presented. Basically, there are two areas regarding the stiffness problem in the configuration of the existing antenna. The first stiffness consideration is with the structureal tie between the back-up structure of the dish and the declination axis torque tube assembly. The second stiffness requirement is the degree of fixity of the spars at their ties to the back-up structure of the antenna. The latter is believed to be the cause of an additional 3/4 minute of arc error on the present structure when an additional 30 pounds is applied near the horn ring. Technically, this is rather conclusive due to the order of magnitude of the deflection of the spars under their own weight as compared with the deflection caused by 50 pounds near the horn ring.

The new antenna will have pie-shaped reflector panels. With respect to the matching of panels and the true significance of the tolerances they proposed to hold in the assembly, D.S. Kennedy went to considerable length to assure us of their capability to meet the requirements. A representative segment of a 28-foot antenna was set up and machined. A set of the optical measurements was submitted to Ewen Knight. The data shows the greatest deviation (.008") from the ideal curve to be at the tip of the panel (the vertex of the reflector). All other points plotted are .005" or under. A value of .00224 inch rms was obtained along the horizontal radius (consider the panel lying on its side); on a plane 3 feet above the horizontal plane the error was .011" rms. Since the panel becomes smaller as the outer rim is approached, it is reasonable to assume the rms value will not differ significantly from these two values. The above remarks are conservative and fairly representative of the overall antenna. In fact, the rms value of the machined panel taking an rms average of all the points reported turns out to be .003". This calculation is based on fifty-three measurements.

Antenna Counterweights

The problem of counterweights is easily solved for the new antenna, since the center of mass of the new antenna has been appropriately located. The plan is to balance the antenna independent of the receiver and front end weights. This allows a variable weight to be either in the front end or in the receiver. This can be accomplished by adding a pipe-tee extension to the counterweight booms both in hour angle and about the declination axis. Removable weights of about 50 lbs. each have been prescribed and can be easily handled. A size of 1" x 10" x 17" would approximate this weight in steel or cast iron.

Comments Relative to the Pedestal

Since the beamwidths at the operating frequencies are 2 and 4.2 mins., the inductosyn readout system must be recalibrated and adjusted. Ferrand, Inc., New York City, will be contacted for this work. The effect of the gear teeth error is on the order of 1 min. of arc. Wear and use of the present system has probably increased this to 2.0 mins. of arc. This readout system accuracy will be adequate for the program after adjustment and recalibration .

Antenna Fit Inside Present Radome

The antenna with spars and horn ring located 1 foot behind the focal plane will fit inside the present 49-foot radome. The comparison antenna must be flush with the front of the horn ring, and its feed must not extend more than 8 inches forward for clearance beneath the radome.

1.2 Manufacture

The parabola was manufactured by the D.S. Kennedy Company, Cohasset, Massachusetts. The structure is that of their standard 28-foot diameter reflector. Some additional structure was added for stiffening purposes. This structure is normally shipped in sections. Since, for the purposes of this contract, the parabola would be shipped in two halves, the unused bolted joints were welded up. Provision for accurate alignment of the two halves was made by appropriate fitted surfaces at the diametral parting line and by the use of close fitting bolts. New frames for attaching the parabola to the sidereal mount, a new feed support ring and spars, and a new counterweight arrangement were constructed.

Fiber board was applied to the rear face of the existing screen on the parabola surface so that approximately half the circumference of the structural tubing which directly supports the screen, would be covered by the foam leaving the other half exposed to the air. Urethane foam of approximately 3 pounds per cubic foot was then sprayed on the front of each half of the parabola to a thickness of about 3 inches. A series of machining operations was then carried out on one half to eliminate excess material. At this point it was found that a few spots did not clean up. These were repaired. Provision on the parabola was made for the attachment of twenty indicator rods. These rods were bolted through holes in the main structural tubes and were mounted approximately parallel to the parabola axis. After the roughing cuts had been completed, both halves were again bolted together and a plane established approximately 6 inches beyond the aperture by scribing marks on these rods. This plane was used to obtain proper relationships in the machining fixture. Final machining of each half was then accomplished separately, a reflecting coat of zinc sprayed on, and a protective finish coat applied to the zinc coat. Initial inspection operations were carried out at this point.

The actual machining operations were carried out by a so-called pendulous routing technique. A milling cutter approximately 8 inches in diameter was mounted on the shaft of a suitable motor and the motor attached to a long tube which was equipped with a gimbal pivot at the opposite end. The length of the tube and the location of the gimbal pivot were adjustable. With this arrangement for a given length of tube and a given position of the gimbal pivot, the cutter generates a spherical surface as it is traversed over the work. A schedule of tube lengths and pivot locations was computed so that a succession of such cuts would approximate the desired parabolic surface. The criteria used in the machining schedule were that the spherical cut was tangent to the desired parabola at the center of the usable zone and that the height at the intersection of two successive spherical zones was not more than .001 inches high. Due to head room limitations in the factory, only one half of the parabola could be machined at one time.

A good deal of difficulty was experienced with proper suspension of each half in the machining fixture and with maintenance of uniform temperature over the entire half of the dish structure. The suspension method finally used involved supporting the parabola half being machined from the two normal pickup points and applying suitable jacks to force the shell into such a position that the scribed lines on the indicator rods fell within a few thousands of one plane. Uniform temperature was attained by closing off that section of the factory and providing a separate heating system for the area. In addition, plastic sheeting was applied to the parabola structure to enclose all its members. Two fans were placed in the enclosure to keep the air inside well stirred.

During the manufacturing period, deflection tests on the structure had indicated that excessive deflection would be encountered with the three spar feed supports specified. Accordingly, the spar configuration was altered to one having four spars.

Each of these four attached to primary structure which connected directly to the four parabola mounting feet. Use of three spars would have required attaching one spar to secondary structure and would have resulted in relatively large deflection not only of the feed, but of the parabola surface as well. In addition, four holes were machined through the parabola surfaces so that the spars could be connected directly to the four mounting feet if rim deflection subsequently proved to be excessive.

1.3 Installation

After both halves had been machined, they were shipped to the Test Site. The balloon was removed from the house, the old parabola taken off in sections, and stored in the yard. The two halves of the new parabola were assembled while still on the ground. During installation of the new A frames, some physical interferences were encountered and corrected. After this was accomplished, the mount was pointed at the zenith and the parabola lowered in place. At this point two interferences were noted between the A frames and two supplementary members which had been added to the structure. It was necessary to cut these tubes and weld them into new locations. Alignment of the mounting bolt holes required some filing before proper fit was obtained. The balloon was reinstalled and inflated. Counterbalances were installed and adjusted by measuring the voltage drop across the filter in series with each axis drive motor. The declination axis counterbalance weights were checked for equality by pointing the antenna at the zenith and rotating the mount about the polar axis in both directions. The declination axis counter balances were checked for proper balance by pointing the antenna at the horizon with the declination axis horizontal and rotating the mount about the declination axis in both directions. In all cases the voltage drop measured across the filter for both directions of rotation were essentially equal. After installation was complete, the measuring rods were removed and stored at the Test Site for possible future use.

1.4 Inspection

Inspection was carried out substantially in accordance with the requirements of Specification #SS-006. The first inspection operations were carried out with the parabola pointing at the zenith. The technique used measured the deviation of the scribed marks on each of the twenty gage rods from a plane. Since the marks on these rods were originally in one plane, and were forced into a plane when the parabolas were machined, the best parabola would be obtained when the rod markings had the same relation to each other that existed in the machining fixture.

Alteration of individual rod deviations was carried out by appropriately shimming each mounting pad and by installation of a jack at the parabola vertex. Shimming was concerned both with the relative level of the mounting feet and with the twisting moments applied to each. The effect of a particular adjustment in shim thickness was obtained by trial. After reasonable progress had been made, the parabola was pointed at the horizon and the measurements repeated. The instrumentation for measuring rod locations while pointing at the horizon gave considerable trouble. The final solution involved use of a milling machine table together with the sighting unit used for setup at the factory. A precision level mounted on the table provided a check on possible deflection of the floor. During these operations examination of the residual distortion indicated that elimination of the interference discovered at the time of installation had introduced measurable distortion of the parabola. Accordingly, provisions were made to permit adjustments to the length of the two members involved.

Considerable difficulty with thermal gradients inside the radome was experienced. The solution to this difficulty was to turn on the furnace blower (without heat) and to add a number of large centrifugal blowers on the opposite side of the radome arranged with their outlets pointing upward. With this arrangement, ΔT for a thermometer at the rim of the dish while it was pointing upward, a thermometer at the top of the concrete pedestal, and a thermometer at eye level was about two degrees with the inside ambient temperature at $90^{\circ}F$.

A weight of about 56 pounds was clamped to the outer surface of the horn ring. After several successive measurements and adjustment sequences had been accomplished, attempting to get the best balance between errors measured while pointing at the zenith and while pointing at the horizon, a final set was taken in each position. These readings were subjected to the analysis described in SS-006. The root mean square error was determined to be .008 inches in the zenith pointing position and .013 inches in the horizon pointing position.

One deviation from the procedure was made. SS-006 specifies that rod mark deviations shall be measured from a plane through the marks on rods a, b, and c. These three rods are located in the central portion of one half of the parabola. Computation of rod errors from this plane results in relatively large deviations which are subject to relatively large error since they are based on extrapolation. It was felt that a better procedure would be to determine errors from the plane which best fitted the measured rod mark positions. In correcting the measured rod position for the initial position of the rods at the time of machining, it was assumed that this plane of best fit corresponded to the instrument plane from which the machining setup was made.

The following discussion pertains to inspection for the items of the purchase specification MPM-025.

1. Zinc coating thickness (.003 minimum): No means of measurement. Considered acceptable.

2. "Focal length 144 inches," no tolerance specified. The surface measuring method used determined the errors from a parabola having a focal length of 144.000 ± 001 inches. Considered acceptable.

3. "Surface tolerance under static condition shall not exceed .020 rms from the theoretical curve when the antenna is mounted in the vertical position and

facing the horizon and also when the antenna is facing the zenith." The errors measured were as follows:

a. Pointing at horizon - .013" rms

b. Pointing at zenith - .008" rms

Considered acceptable.

4. "The antenna shall have four aluminum spars located at 45° off the axis of the dish and shall extend forward of the focal plane 12 inches to the centerline of the horn ring. A horn ring with an opening of 15 inches square shall be provided-------." This specification requirement was modified by Memo #MPM-042 to permit three spars and subsequently by Memo #MPM-050 to require four spars spaced at 60°, 120°, 60°, and 120°. This latter requirement is considered to have been met.

5. "The deflection of these four spars under their own weight, plus a package weighing 50 pounds, shall not exceed .010 inches along the boresight axis when the dish is mounted in a vertical position and facing the horizon." This was later increased to .013 inches (MPM-042). There was no means of measuring for this requirement. Considered acceptable.

6. "These spars are to be attached to the dish structure in such a way as to not distort the surface from the ideal curve." It is not clear as to exactly what this means. There was no means of verifying how the

attachment distorted the parabola. The deflections of the parabola surface, due to loads applied at the attachment points, met the rms requirements specified. The present construction is considered acceptable.

7. "The gross weight of the antenna shall not exceed 2250 pounds and a design goal of less than 2000 pounds is desirable." The maximum weight requirement was relaxed to 2325 pounds (MPM-042). The parabola less spars and horn ring weighed 2000 pounds. This requirement is considered to have been met.

8. "A 3-inch circular hole at the vertex shall be provided and 3 holes 1/4 inch in diameter equally spaced around this cutout shall be provided, as well as a vertex mounting plate and attaching hardware." Considered acceptable, although there was no "vertex mounting plate and attaching hardware."

9. "In the event the radome should fail, the antenna shall be able to withstand loads resulting from winds of 100 mph and 2 inches of ice without any permanent deformation." There was no means of checking this. Considered acceptable.

10. "The primary support structure shall not extend more than 16 inches behind the vertex -----." Considered acceptable, although an additional tie between the parabola structure and the mount was installed at the vertex.

11. The A frame structure shall point the antenna with an accuracy better than 1 minute of arc. There was no means of checking this. Considered acceptable.

12. "About both axes provide counterweight balancing the antenna within 200 pound-feet and adjustable to balance primary feed systems weighing from 5 pounds to 100 pounds." Considered acceptable.

13. "Insulate O.D. of spars." Analysis of heat transfer considerations as they affect temperature distribution and thermal distortion of the mount indicate that all parts of the structure should be at the same temperature. Therefore, thermal insulation of the spars was considered undesirable, and this requirement waived.

14. "Boresight horn ring within .020." The specification is not clear as to what the horn ring is boresighted to or what constitutes the reference. The antenna was pointed at the zenith as determined by the plane of the scribed marks on the measuring rods. A plumb line dropped from the approximate center of the horn ring was within 1/8 inch of the center of the 3-inch circular hole. This is considered acceptable.

15. During the rigging operations a few pieces of foam were chipped off the edges of the parabola. This is considered to be of no moment.

16. In summary, the antenna is considered to have met the requirements of the specification in all essential details.

The following computational steps were carried out for the antenna pointing at the horizon and again for the antenna pointing at the zenith.

1. Using the optical micrometer measurements of rod mark positions with respect to the measuring instrument plane, the parameters (a, b, c,) of the plane ($Z = Ax + By + C$) which best approximated this data on an rms basis were computed.

2. The displacement ($M - Z$) of each rod mark from the rms plane was computed.

3. The values of ($M - Z$) were corrected for the initial position of the rod mark at the time of machining. This remainder (C_a, C_b, C_c --- C_t) was considered to be the displacement of the rod mark between its position at the time of machining and its position after the antenna was installed.

4. The displacement of the surface at each surface measurement point was computed by linear interpolation using the mark displacements determined in Paragraph 3. Derivation of the interpolation equations is contained in the computations at the end of the Report. The coefficients for each point are listed in SS-006.

5. The surface measurement point displacements computed in Step 4 were added to the surface errors determined when the parabola was still in the machining fixture. The result of each computation was squared, the squares summed, the

sum divided by the number of surface measurement points considered, and the square root extracted to give the rms error.

6. Computations for Steps 1, 2, and 3 are included in this report. The derivation of the rms plane parameters is also included.

7. The location of the mark on rod "p" was obscured by the spar when the parabola was pointing vertically. Although computations for the location of the rms plane were carried out without this mark location, it was decided, for computation of the rms surface error, to estimate its location on the basis that the change in deflection with respect to the neighboring rods when moving from zenith pointing to horizon pointing would be similar to that for rod "h" and its companions. This computation is shown in pages 19 through 27.

COMPUTATION OF C_a,

ANTENNA POINTINC

Point	x	y	Optical Micrometer Reading (inches) = M	Mx	My	A B C Ax
a	0	+ .06	-.035	0	-.0021	0 + .0(
b	+ .93	+1.62	-.034	-.0316	-.0551	-.0004 + .0(
c	- .93	+1.62	-.008	+.0074	-.0130	-.0004 + .0(
d	+3.50	+ .37	-.014	-.0490	-.0052	-.0017 + .0C
e	+2.51	+2.50	-.014	-.0351	-.0350	-.0012 + .00
f	+1.53	+3.18	-.004	-.0061	-.0128	-.0007 + .00
g	+ .28	+3.53	0	0	0	-.0001 + .0
h	-1.37	+3.25	-.013	+.0178	-.0423	-.0007 + .00
i	-2.50	+2.50	-.002	+.0050	-.0050	+.0012 + .00
j	-3.50	+ .37	+.003	-.0105	+.0011	+.0017 + .00
k	0	- .06	-.035	0	+.0021	0 - .00(
l	- .93	-1.62	-.022	+.0206	+.0356	+.0004 - .00
m	+ .93	-1.62	-.029	-.0270	+.0469	-.0004 - .00
n	-3.50	- .37	+.003	-.0105	-.0011	+.0017 - .001
o	-2.50	-2.50	-.028	+.0700	+.0700	+.0012 - .007
p	-1.53	-3.18	-.053	+.0813	+.1685	+.0007 - .009
q	- .28	-3.53	-.031	+.0082	+.1093	+.0001 - .010
r	+1.37	-3.25	-.013	-.0178	+.0423	-.0007 - .009
s	+2.50	-2.50	+.005	+.0125	-.0125	-.0012 - .007
t	+3.50	- .37	-.014	-.0490	+.0052	-.0017 - .001
			Σ = -.338	Σ = -.0387	Σ = +.2949	

COMPUTATION OF C_a, C_b, C_c ---- C_t

ANTENNA POINTING AT HORIZON

A = -.000477
B = +.002836
C = -.0169

My	Ax + By + C = Z	(M-Z)	Rod Error Measured At Time of Machining (R)	(M - Z) - R
-.0021	0 + .0002 - .0169 = -.0167	-.018	+.002	-.020 = C_a
-.0551	-.0004 + .0047 - .0169 = -.0126	-.021	-.003	-.018 = C_b
-.0130	-.0004 + .0047 - .0169 = -.0126	+.005	+.001	+.003 = C_c
-.0052	-.0017 + .0011 - .0169 = -.0175	+.003	0	+.003 = C_d
-.0350	-.0012 + .0072 - .0169 = -.0109	-.003	+.003	-.006 = C_e
-.0128	-.0007 + .0092 - .0169 = -.0084	+.004	-.005	+.009 = C_f
0	-.0001 + .0102 - .0169 = -.0068	+.007	+.004	+.003 = C_g
-.0423	-.0007 + .0094 - .0169 = -.0082	-.005	-.002	-.003 = C_h
-.0050	+.0012 + .0072 - .0169 = -.0085	+.007	+.002	+.005 = C_i
+.0011	+.0017 + .0011 - .0169 = -.0141	+.017	-.002	+.019 = C_j
+.0021	0 - .0002 - .0169 = -.0171	-.018	0	-.018 = C_k
+.0356	+.0004 - .0047 - .0169 = -.0212	-.001	0	-.001 = C_l
+.0469	-.0004 - .0047 - .0169 = -.022	-.007	0	-.007 = C_m
-.0011	+.0017 - .0011 - .0169 = -.0163	+.019	0	+.019 = C_n
+.0700	+.0012 - .0072 - .0169 = -.0229	-.005	+.003	-.008 = C_o
+.1685	+.0007 - .0092 - .0169 = -.0254	-.028	0	-.028 = C_p
+.1093	+.0001 - .0102 - .0169 = -.0270	-.004	+.005	-.009 = C_q
+.0423	-.0007 - .0094 - .0169 = -.0270	+.014	-.008	+.022 = C_r
-.0125	-.0012 - .0072 - .0169 = -.0253	+.030	+.002	+.028 = C_s
+.0052	-.0017 - .0011 - .0169 = -.0197	+.006	-.002	+.008 = C_t

$\sum$ = +.2949

2

ANTENNA POINTING AT HORIZON

Computation of RMS Plane Coefficients

$$Z = Ax + By + C$$

$$\sum Mx = -.0387$$

$$\sum My = +.2949$$

$$\sum M = -.338$$

$$A = .010206 \sum Mx - .000274 \sum My$$

$$= .010206 (-.0387) - .000274 (+.2949)$$

$$= -.000396 - .0000807$$

$$= -.000477$$

$$B = -.000278 \sum Mx + .00975 \sum My$$

$$= -.000278 (-.0397) + .00975 (.2949)$$

$$= +.00001075 + .002875$$

$$= +.002886$$

$$C = .05 \sum M$$

$$= .05 (-.338)$$

$$= -.01690$$

COMPUTATION OF C_a, C_b, C_c

ANTENNA POINTING AT ZE

A = -.0
B = +.0
C = -.0

Point	x	y	Optical Micrometer Reading (Inches) = M	Mx	My	Ax + By
a	0	+ .06	-.030	0	-.0018	0 + 0 -.
b	+ .93	+1.62	-.056	-.0521	-.0907	-.00507 + .00140 - .
c	- .93	+1.62	-.037	-.0344	-.0600	+.00507 + .00140 - .
d	+3.50	+ .37	-.066	-.2310	-.0244	-. 0191 + . 0003 - .
e	+2.51	+2.50	-.066	-.1655	-.1650	-. 0137 + .00216 - .
f	+1.53	+3.18	-.055	-.0843	-.1750	-.00836 + .00275 - .
g	+ .28	+3.53	-.026	-.0073	-.0918	-.00153 + .00305 - .
h	-1.37	+3.25	-.030	+.0410	-.0975	+.00748 + .00281 - .
i	-2.50	+2.50	-.022	+.0550	-.0550	+.01366 + .00216 - .
j	-3.50	+ .37	-.027	+.0943	-.0100	+. 0191 + . 0003 - .
k	0	- .06	-.030	0	+.0018	0 0 -..
l	- .93	-1.62	-.026	+.0242	+.0422	+.00507 - .00140 - .
m	+ .93	-1.62	-.041	-.0382	+.0665	-.00507 - . 0014 - .
n	-3.50	- .37	-.027	+.0943	+.0100	+. 0191 - . 0003 - .
o	-2.50	-2.50	-.009	+.0225	+.0225	+.01366 - .00216 - .
p	-1.53	-3.18	----	----	----	---- ----
q	- .28	-3.53	-.016	+.0045	+.0565	+.00153 - .00305 - .
r	+1.37	-3.25	-.041	-.0562	+.1336	-.00748 - .00281 - .
s	+2.50	-2.50	-.034	-.0852	+.0852	-.01366 - .00216 - .
t	+3.50	- .27	-.066	-.2310	+.0244	-. 0191 - . 0003 - .
			$\sum$ = -.705	$\sum$ = -.5806	$\sum$ = -.0225	

1

COMPUTATION OF C_a, C_b, C_c ---- C_t

ANTENNA POINTING AT ZENITH

A = -.005458
B = +.000864
C = -.036838

My	Ax + By + C = Z	(M-Z)	Rod Error Measured At Time Of Machining (R)	(M - Z) - R
-.0018	0 + 0 -.03684 = -. 0368	+.007	+.002	+.005 = C_a
-.0907	-.00507 + .00140 - .03684 = -. 0405	-.015	-.003	-.012 = C_b
-.0600	+.00507 + .00140 - .03684 = -. 0304	-.007	+.001	-.008 = C_c
-.0244	-. 0191 + . 0003 - .03684 = -. 0556	-.010	0	-.010 = C_d
-.1650	-. 0137 + .00216 - .03684 = -. 0484	-.018	+.003	-.021 = C_e
-.1750	-.00836 + .00275 - .03684 = -. 0425	-.012	-.005	-.007 = C_f
-.0918	-.00153 + .00305 - .03684 = -. 0353	+.009	+.004	+.005 = C_g
-.0975	+.00748 + .00281 - .03684 = -.02655	-.003	-.002	-.001 = C_h
-.0550	+.01366 + .00216 - .03684 = -.02102	-.001	+.002	-.003 = C_i
-.0100	+. 0191 + . 0003 - .03684 = -.01742	-.010	-.002	-.008 = C_j
+.0018	0 0 -..03684 = -. 0368	+.007	0	+.007 = C_k
+.0422	+.00507 - .00140 - .03684 = -. 0332	+.007	0	+.007 = C_l
+.0665	-.00507 - . 0014 - .03684 = -. 0433	+.002	0	+.002 = C_m
+.0100	+. 0191 - . 0003 - .03684 = -. 0181	-.009	0	-.009 = C_n
+.0225	+.01366 - .00216 - .03684 = -. 0253	+.016	+.003	+.013 = C_o
--	---- ---- ---- ----	----	0	---- = C_p
+.0565	+.00153 - .00305 - .03684 = -. 0384	+.022	+.005	+.017 = C_q
+.1336	-.00748 - .00281 - .03684 = -. 0471	+.006	-.008	+.014 = C_r
+.0852	-.01366 - .00216 - .03684 = -. 0527	+.019	+.002	+.017 = C_s
+.0244	-. 0191 - . 0003 - .03684 = -. 0563	-.010	-.002	-.008 = C_t
-.0225				

2

ANTENNA POINTING AT ZENITH

Computation of RMS Plane Coefficients

$$Z = Ax + By + C, \qquad \sum Mx = -.5806$$

$$\sum My = -.0225$$

$$\sum M = -.705$$

$$A = 2.63711 \times 10^{-4} \times \sum My - 8.8712 \times 10^{-4} \sum M + 1.046878 \times 10^{2} \sum Mx$$

$$= (2.637)(-.0225) \times 10^{-4} - 8.8712 \times 10^{-4} (-.705) + 1.0468 \times 10^{-2} (-.5806)$$

$$= (-.00593 + .6254 - 6.078) \times 10^{-3}$$

$$A = -.005458$$

$$B = 1.0897 \times 10^{-2} \sum My - 1.8462 \times 10^{-3} \sum M + 3.308 \times 10^{-4} \sum Mx$$

$$= 1.0897 \times 10^{-2} (-.0225) - 1.8462 \times 10^{-3} (-.705) + 3.308 \times 10^{-4} (-.5806)$$

$$= (-.2452 + 1.3016 - .1921) \times 10^{-3}$$

$$= +.000864$$

$$C = -1.8240 \sum My \times 10^{-3} + 5.3042 \sum M \times 10^{-2} - 8.8716 \sum Mx \times 10^{-4}$$

$$= -1.824 \times 10^{-3} (-.0225) + 5.3042 \times 10^{-2} (-.705) - 8.8716 \times 10^{-4} (-.5806)$$

$$= (+ .04104 - 37.39489 + .51509) \times 10^{-3}$$

$$= -.036838$$

DERIVATION OF EQUATIONS DEFINING A PLANE APPROXIMATING A NUMBER OF POINTS IN A THREE DIMENSIONAL SYSTEM ON AN RMS BASIS

Equation of Plane

$$Z = Ax + By + C$$

Let $(x_1 y_1 M_1), (x_2 y_2 M_2)$ ----- $(x_n y_n M_n)$ be the coordinates of the points considered for any point in the system.

$$(Z - M)^2 = (Ax + By + C - M)^2$$
$$= A^2x^2 + B^2y^2 + C^2 + M^2 + 2ABxy + 2ACx - 2AMx + 2BCy - 2MBy - 2MCx$$

For all Points in the System

$$S = \sum_{n=1}^{n} (Z_n - M_n)^2 = A^2 \sum_{n=1}^{n} x_n^2 + B^2 \sum_{n=1}^{n} y_n^2 + {}_nC^2 + \sum_{n=1}^{n} M^2 + 2AB \sum_{n=1}^{n} x_n y_n$$

$$+ 2AC \sum_{n=1}^{n} x_n - 2A \sum_{n=1}^{n} M_n x_n + 2BC \sum_{n=1}^{n} y_n - 2B \sum_{n=1}^{n} M_n y_n - 2C \sum_{n=1}^{n} Mx$$

For S to be a Minimum

$$\frac{\partial S}{\partial A} = 0 = 2A \sum x_n^2 + 2B \sum x_n y_n + 2C \sum x_n - 2 \sum M_n x_n$$

$$\frac{\partial S}{\partial B} = 0 = 2B \sum y_n^2 + 2A \sum x_n y_n + 2C \sum y_n - 2 \sum M_n x_n$$

$$\frac{\partial S}{\partial C} = 0 = 2nC + 2A \sum x_n + 2B \sum y_n - 2 \sum Mx$$

FOR THIS PARABOLA WITH THE PRESENT ROD POSITIONS POINTING AT HORIZON. ALL RODS ARE VISIBLE

$$\Sigma x = 0$$
$$\Sigma y = 0$$
$$\Sigma x^2 = 98.052$$
$$\Sigma y^2 = 102.788$$
$$\Sigma xy = 2.80$$

Substituting these values in the equations for

$$\frac{\delta S}{\delta A}, \quad \frac{\delta S}{\delta B}, \quad \frac{\delta S}{\delta C}$$

results in a set of simultaneous equations:

$$196.104\,A + 5.60\,B - 2\,\Sigma Mx = 0$$
$$5.60\,A + 205.576B - 2\,\Sigma My = 0$$
$$40.0\,C - 2\,\Sigma M = 0$$

Solving simultaneously

$$A = .010206\,\Sigma Mx - .000274\,\Sigma My$$
$$B = -.000273\,\Sigma Mx + .00975\,\Sigma My$$
$$C = \frac{\Sigma M}{20}$$

FOR THIS PARABOLA WITH THE PRESENT ROD POSITIONS, POINTING AT THE ZENITH ALL RODS EXCEPT ROD P ARE VISIBLE

$$\Sigma x = + 1.53$$
$$\Sigma y = + 3.18$$
$$\Sigma x^2 = 95.712$$
$$\Sigma y^2 = 92.338$$
$$\Sigma xy = - 2.06$$

Substituting These Values in the Expressions for $\frac{\delta s}{\delta A}$, $\frac{\delta s}{\delta B}$, $\frac{\delta s}{\delta C}$ gives

$$191.424\,A - 4.12\,B + 3.06\,C - 2\sum Mx = 0$$

$$-4.12\,A + 184.676\,B + 6.36\,C - 2\sum My = 0$$

$$+3.06\,A + 6.36\,B + 38.0\,C - 2\sum M = 0$$

Solving Simultaneously

$$A = .0002637\sum My - .000887\sum M + .010469\sum Mx$$

$$B = +.0108978\sum My - .00184618\sum M + .0003308\sum Mx$$

$$C = -.001824\sum My + .05304\sum M - .000887\sum Mx$$

EXPLANATION OF COMPUTATIONS TO ESTABLISH POSITION OF ROD P IN VERTICAL POINTING POSITION

NOTE: g, h, i, are symmetrical with o, p, q, and are affected by similar loads

ROD	ROD LOCATION RELATIVE TO INSTRUMENT PLANE		Δ
	HORIZONTAL	VERTICAL	(HOR-VERT)
g	+ .003	+ .005	-.002
h	- .008	- .001	-.007
i	+ .005	- .003	+ .008
o	- .007	+ .013	- .020
p	- .027	?	?
q	- .009	+ .017	-.026

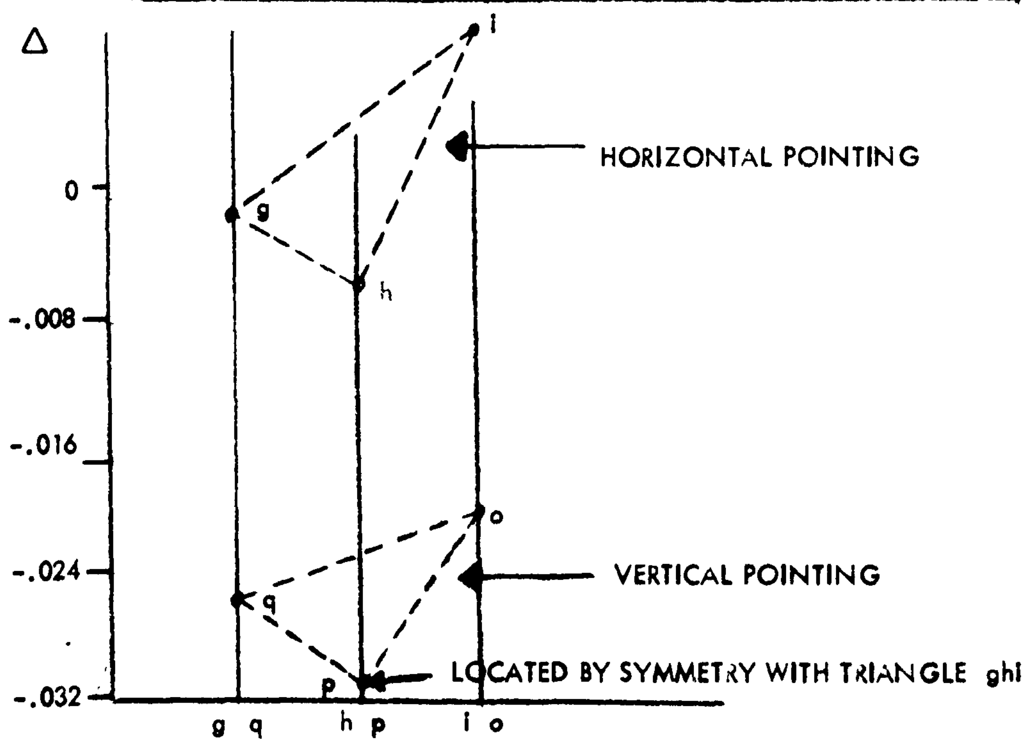

Thus Δ_p = -.031, Rod location (Vert.) = -.027 - (-.031) = + .004

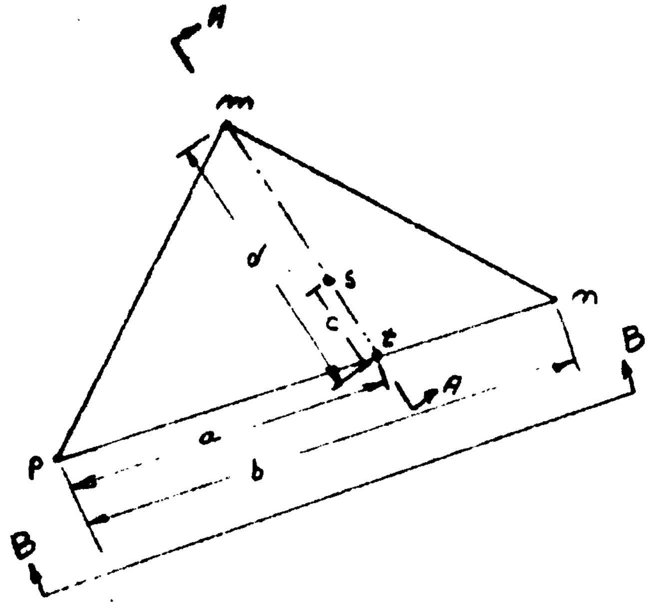

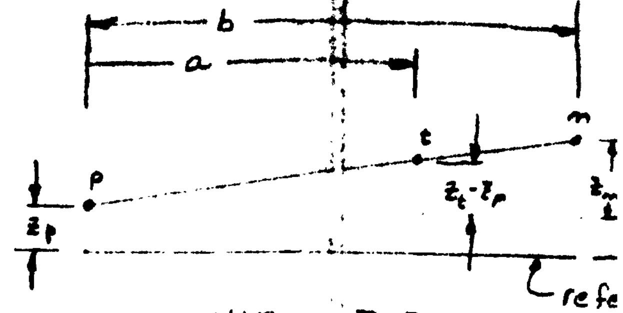

VIEW B B

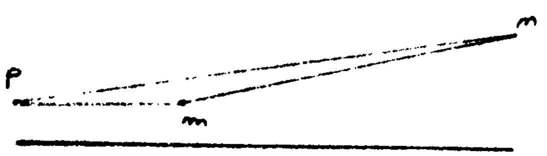

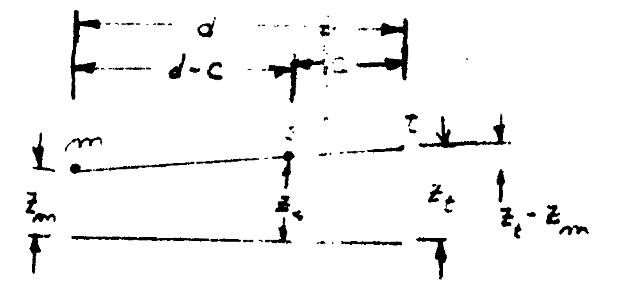

$$z_s = \frac{d-c}{d}\left[\frac{a}{b}(z_n - z_p) + z_p - z_m\right] + z_m$$

$$= z_m\left[1 - \frac{d-c}{d}\right] + z_n\left[\left(\frac{d-c}{d}\right)\left(\frac{a}{b}\right)\right] + z_p\left[\left(\frac{d-c}{d}\right)\left(-\frac{a}{b}\right) + \frac{d-c}{d}\right]$$

$$1 - \frac{d-c}{d} = \frac{c}{d} \;;\; \left(\frac{d-c}{d}\right)\left(\frac{a}{b}\right) = \left(1 - \frac{c}{d}\right)\left(\frac{a}{b}\right) \;;\; \left(\frac{d-c}{d}\right) - \frac{d-c}{d}\left(\frac{a}{b}\right) = \left(1 - \frac{c}{d}\right)\left(1 - \frac{a}{b}\right)$$

$$z_s = z_m\left(\frac{c}{d}\right) + z_n\left(1 - \frac{c}{d}\right)\left(\frac{a}{b}\right) + z_p\left(1 - \frac{c}{d}\right)\left(1 - \frac{a}{b}\right)$$

a, b, c, d, determined graphically for each point.

Check: $\frac{c}{d} + \left(1 - \frac{c}{d}\right)\frac{a}{b} + \left(1 - \frac{c}{d}\right)\left(1 - \frac{a}{b}\right) \equiv 1$

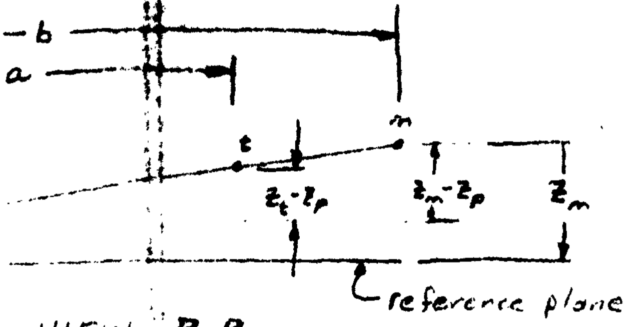

VIEW B B

$$\frac{z_m - z_p}{b} = \frac{z_t - z_p}{a}$$

$$z_t = \frac{a}{b}(z_m - z_p) + z_p$$

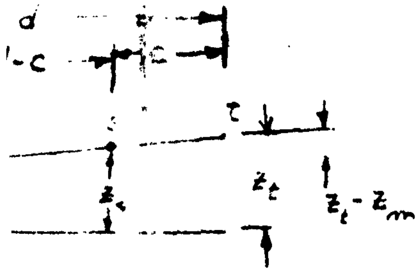

$$\frac{z_t - z_m}{d} = \frac{z_s - z_m}{d-c}$$

$$z_s = \frac{d-c}{d}(z_t - z_m) + z_m$$

$-c\,]$

$\left(\frac{a}{b}\right) = \left(1 - \frac{c}{d}\right)\left(1 - \frac{a}{b}\right)$

$)$

... point.

DETERMINATION OF
INTERPOLATION
COEFFICIENTS

Appendix

2.0 FEED POSITIONING SUBSYSTEM

2.1 Feed Positioning Device Design

The exact position of the RF feed horn with respect to the focal point of the operating antenna is an important consideration in this program because of the millimeter wavelengths of the signals to be observed. Ewen Knight has considered many different approaches to the feed positioning problem, some of which were completely automatic and were thus prohibitive in cost. The focusing device must be developed and installed compatibly with the horn ring, the spar assembly and the front end RF component package.

2.1.1 Positioning Methods

Positioning devices fall into two categories: those which move the feed with respect to the focal point and those which move the focal point with respect to the feed. Several methods for moving the feed with respect to the focal point have been studied; one method of moving the focal point with respect to the feed was considered. Possible methods for moving the feed include:

A. Spar pressurization

B. Spar temperature control

C. Movable platform

Spar pressurization was determined to be feasible for relatively small movements only, if reasonable pressure limitations were adhered to. Altering spar length with heaters located inside the spar was feasible but the relatively long response time of such a system made it undesirable. Both of these systems are capable in principle of controlling the feed position along as well as perpendicular to the boresight axis.

Schemes for positioning <u>only</u> the primary horn were rejected. No flexible waveguide is available at 75 Kmc and elastic flexure of rigid waveguide over the selected travel would require 3 feet of unsupported waveguide between the primary horn and the ferrite switch for 75 Kmc and 4 feet of waveguide for 35 Kmc. This would result in attenuations at this location alone of 2.7 and .9 db respectively.

The primary feed points in the direction of the target; a splash plate reflects the energy focused by the parabola into the feed horn. Advantages of this system are the relatively small mass which must be moved to achieve focusing the increased clearance then available between the reflected focal point and radome. The disadvantages are the relatively unknown performance of such a system with respect to side lobes, losses, etc.

A movable platform with only one degree of freedom in translation was selected as the most feasible approach. This device will consist of two plates one of which can be moved with respect to the other. The stationary plate will be adjustably attached to the spar ring. This adjustment, to position the equipment roughly, will be made and locked. The radiometer focal point equipment will be mounted to the movable plate. An arrangement of three ball bearing mounted eccentrics properly phased together at assembly and maintained in phase by two worm gears will provide for movement of the top plate. A motor coupled through a suitable gear reduction will afford remote control. Position indication will be accomplished through a synchro coupled to the drive worm. A follow-up synchro, located at the operator's station, and gear coupled to a counter will provide position information to the operator. This method of positioning avoids all limit stop problems and the use of linear translating devices which are subject to binding under non-central loading. Some small offset perpendicular to the boresight axis is introduced by this method of focusing. However, this can be calibrated out for any given indicated position and by judicious design and initial setting the calibration will be kept to a minimum.

2.2 Feed Positioning Device Fabrication

The adjustable feed system is accomplished by the design of a movable plate and carriage mounted on the horn ring of the antenna. A mockup of this ring along with its supports was to be used for testing purposes in the Laboratory prior to actual installation at the site. The carriage assembly is composed of a fixed plate 19 inches square fastened to the horn ring. On this plate is mounted a drive motor, a series of housings, three of which contain a drive, screw, and sprocket. The sprockets are then surrounded by a roller chain. Another plate 19 inches square, containing three nut assemblies, is mounted to the drive screws. When the motor is energized, motion is transmitted through the sprocket chain and drive screws to the plate containing the nut assemblies allowing it to have a total forward and reversible movement of about $\pm$ 0.5 inch. Microswitches are mounted at each limit to de-energize the motor. The position of the movable plate is determined by the use of a selsyn mounted on the carriage and also on the control panel of the control console. A suitable dial calibrated in 1,000 steps will be mounted on the face of the control panel. The operation of the carriage will also be remotely controlled by the addition of a forward and reverse switch.

2.3 Feed Positioning Device Testing

The feed position is adjusted along the antenna boresight axis by means of a fixed plate and a motor driven carriage. The fixed plate is mounted on the antenna horn ring. A drive motor, mounted on the fixed plate, engages three drive screws through a chain and sprocket arrangement. The movable carriage contains three captive nut assemblies which mate to the drive screws. When the motor is actuated the movable carriage is driven along the antenna boresight axis through a maximum travel of one inch. The motor is automatically de-energized by limit switches at the extremes of the carriage excursion. A synchro mounted on the carriage is used to provide positional data to a corresponding unit on the control console which drives a counter providing a readout resolution of 0.001 inch.

The feed positioning device was constructed and tested. The fact that no binding occurred during carriage travel verified that the chain and sprocket arrangement achieved its objective. The positioner was operated from the control console and found to be adjustable to the prescribed 0.001 inch.

3.0 RECEIVER SYSTEMS

3.1 Design

Several receiving systems were studied with the chief phase of this study being:

1. Maximum sensitivity for minimum detectable signal.
2. Optimum overall system component parameter trade-offs.
3. The greatest versatility for future modification of the state-of-the-art advances.

An analysis of competing superheterodyne receivers was made to show how the interplay of parameters among many types of RF amplifiers, with varying center frequencies and bandwidths, affected receiver sensitivity. The design of the receivers was based on the outcome of this initial analysis.

Some of the other considerations in the 8 mm portion of the receiver systems was that the introduction of General Electric Z-3040 TWT would be used as a TRF Receiver front end at 35 Gc. Due to unavailability of TWT's at 35 Gc, this effort was stopped. Hence it was decided to forego design of a TRF and commence design on a conventional 35 Gc superhet system similar to that which was proposed for the 75 Gc system which utilized 35 Mc IF system similar to that which was used for the NH3 effort.

3.2 Fabrication and Testing

3.2.1 X-Band System

An X-band system consisting of a tunnel diode followed by a TWT, yielding $0.03^{\circ}K$ rms/second was installed at the Test Site on September 28 primarily for focus location using discrete radio sources. The receiver was completely swamped by radar interference corresponding to temperatures of thousands of degrees Kelvin. Band-rejection filter techniques cannot remedy this situation because of the wide spectrum of radar signals and because of the number of such installations in the immediate area.

Limiting the bandwidth defeats the purpose since the radiometer sensitivity is provided by the wide bandwidth. It appeared that the 9 Gc frequency was an unfortunate choice and a shift to the 7.5 Gc to 8.5 Gc band was made.

The shift in frequency from 9 Gc to 8 Gc involved the following:

a. Laboratory assembly of a ferrite switch with a center frequency of 8 Gc.

b. Because of the unavailability of tunnel diode amplifiers at 8 Gc, two approaches were considered:

    1. The 9 Gc tunnel diodes will be redesigned for an 8 Gc center frequency.

    2. TWT's will be used.

c. Two or more bandpass filters will be necessary to limit the bandwidth to 7.5 Gc to 8.5 Gc to remove the radar interference previously encountered.

From a scientific viewpoint, the X-band measurements by themwelves yield the least information; therefore, the X-band system was given the lowest priority.

3.2.2 <u>35 Gc Channel</u>

The 35 Gc receiver consisted of a conventional 30 Mc IF system using an LEL preamplifier, mixer and IF strip. This system yielded about 5°K rms/second. Further work improved this figure to 1°K rms/second.

3.2.3 <u>75 Gc Channel</u>

A 75 Gc mixer, similar to the WR-28 used at 35 Gc was under development at MDL. However, after approximately three months MDL reported that they had not been able to obtain the bandwidth necessary to take advantage of the X-band IF techniques. Therefore, this mixer was converted into a standard mixer configuration with IF output at 30 Mc. This allowed system assembly and test of a conventional superheterodyne receiver.

APPENDIX

SUMMARY OF VENUS AND LUNAR OBSERVATIONS

TABLE OF CONTENTS

LIST OF FIGURES

LIST OF TABLES

1.0 INTRODUCTION

1.1 Scope of Report

The purpose of this report is to present the scientific findings resulting from work performed under the subject contract from May 1, 1962 to May 1, 1963.

The Report will be broken into two categories:

1. Lunar observing program.
2. Venus observing program.

The description of these programs will include:

1. Purpose of observational program.
2. Method of observation.
3. Method of data reduction.
4. Experimental data.
5. Interpretation of data.
6. Presentation of final results and a discussion of their significance and limitations.

The complete engineering history of the program will not be reported here since such has already been done in the monthly progress reports required by contract.

1.2 Lunar Program

This section will briefly summarize the most significant results of the lunar observing program. The lunar observing program will be described in detail in section 2.0.

Three regions of the lunar surface were chosen for observation. They were:

1. The sub-terrestrial region.
2. Zero degrees selenographic latitude, thirty degrees East selenographic longitude.
3. Zero degrees selenographic latitude, thirty degrees West selenographic longitude.

These three regions are each separated by two antenna beamwidths, and each cover an area on the lunar surface approximately 150 miles in radius. Measurements of temperature at 8.5 mm wavelengths as a function of time indicate that the sub-terrestrial point and the region centered at 30° West longitude appear the same as the average lunar surface. However, the region centered at 30° East longitude appears to be heating and cooling more rapidly than the average lunar surface.

Zero latitude and 30° East longitude is located somewhat South and East of the crater Copernicus, a region that has been observed to remain warmer than its surrounding at infrared wavelengths and to exhibit low reflectivity in millimeter radar measurements.

1.3 Venus Program

In this section the results of the 8.5 mm observations of the planet Venus are summarized. The program will be described in detail in Section 3.0.

For a period of three weeks following conjunction, November 12, 1962, a total of seven days of observation were accumulated before the signal from Venus became obscured by system noise. The last observational attempt, which was unsuccessful, was made on December 18, 1962.

The results of the measurements were:

1. In evident conflict with the Soviet 8.5 mm "phase-effect".
2. In agreement with the recent Mariner microwave data which show no major temperature difference between the light and dark sides of the planet.

The results of this program and a description of the experimental method have been submitted to the Astrophysical Journal for publication. A further more extensive publication will be made after more data analysis and error investigations have been made. Such publications will be submitted to NASA for prior approval.

1.4 Description of Equipment

The system performance parameters at 8.5 mm are summarized below.

Antenna:

Diameter = 28 ft.

Mount - equatorial

Efficiency (excluding radome loss) = 50%

Beamwidth - 4 minutes of arc

Pointing accuracy - 1 minute of arc

Radiometer:

Type - Dicke superheterodyne

Noise figure = 9.3 db

Noise temperature fluctuation (for 1 second time constant) = $1^{\circ}K$ rms

Bandwidth = 20 Mc

Calibrate Signals = $5^{\circ}K$ or $150^{\circ}K$

Data presentation - strip chart recorder

2.0 LUNAR OBSERVATIONAL PROGRAM

2.1 Background

The temperature of the lunar surface is governed by the thermal parameters of the surface material, and by the nature and intensity of the radiation incident upon it. Therefore, the determination of lunar surface and subsurface temperatures provides information concerning the thermal properties of the moon's surface material. This information, in turn, allows one to speculate as to the nature of certain features of the lunar surface. Thus, detailed measurements of temperature variations during periods of known variations in the heat influx at the moon's surface and the theoretical interpretation thereof are of considerable interest.

Various methods are available to measure the temperature variations, the most important being determinations of the radiation emitted by the moon in the infrared and microwave or radio region of the electromagnetic spectrum. A basic difference, however, lends importance to the microwave results: infrared radiation originates primarily on the surface of the moon, while radiation in the microwave region has its origin beneath the surface due to the relative transparency of the lunar surface to microwave radiation.

Previous radio observations of the moon have, with few exceptions, been made with antenna beamwidths which were of the order of a lunar diameter or larger. Such measurements can yield information about the average lunar surface. The interpretation of such measurements is difficult, to say the least; and these measurements, in themselves, provide no information as to the detailed structure of some of the more important lunar features. The 28-foot diameter antenna used in this program has demonstrated a four minute of arc beamwidth at a wavelength of 8.5 mm, the wavelength at which this effort was concentrated. Therefore, the spatial ambiguity inherent in most earlier work was resolved.

2.2 Data Reduction Procedure

The reduction of any experimental observations of surface temperature variations to useful information concerning the lunar surface material requires a theoretical model for comparison. The model selected depends upon the accuracy of the experimental data and the mathematical tools available for the solution.

A theoretical treatment of the temperature variation of the lunar surface and subsurface invariably produces the problem of solving a second-order partial differential equation with nonlinear boundary conditions. Thus, either a simplifying approximation must be made on the boundary conditions such that the problem may be solved analytically, or a numerical method must be employed for the solution with the exact nonlinear boundary conditions. Both approaches have been utilized in previous work (Ref. 1-8).

One approach, useful for analyzing the temperature variations at radio wavelengths, bypasses the problem of nonlinear boundary conditions by obtaining the radio wavelength solution in terms of the infrared temperature variations (Ref. 9-10). Although this method requires knowledge of the infrared temperature variations, it has the advantage of being insensitive to systematic microwave experimental errors and does not, therefore, require knowledge of the lunar surface emissivity or the radio antenna gain characteristics. It is this method that was used for the reduction of lunar data obtained in this program. A brief review of the theory is given in the Appendix.

If the radio temperature is plotted as a function of time, and the resulting waveform harmonically analyzed, it is shown in the Appendix that the ratio of the n^{th} Fourier harmonic amplitude, T'_n, to the average value, T'_o, is given by

$$\frac{T'_n}{T'_o} = \left[1 + 2\delta_n + 2\delta_n^2\right]^{-1/2} \frac{T_n}{T_o}$$

and, the phase of the n^{th} harmonic, ϵ_n, relative to the phase of the infrared n^{th} harmonic by

$$\tan \epsilon_n = \frac{\delta_n}{1 + \delta_n}$$

where:

T_n/T_o = amplitude ratio for the infrared temperature variation.

$$\delta_n = \frac{2\pi n^{1/2}}{\sigma \sec\theta}\left[\frac{\pi P k \epsilon_o K}{\rho c \mu_o}\right]^{1/2}$$

P = lunar orbital period

k = thermal conductivity

K = dielectric constant

ϵ_o = permittivity of free space

μ_o = permeability of free space

ρ = density

c = specific heat

Therefore, from a harmonic analysis of the antenna temperature as a function of time, the amplitude and phase lag of the n^{th} Fourier harmonic relative to those of the infrared temperature variation can be related directly to the δ_n and, information concerning the electrical and thermal parameters of the subsurface material can be deduced. The fundamental frequency of the temperature variation should be used for this analysis since it is the largest and can be more accurately determined.

2.3 The Experimental Procedure

The objective of the experimental part of the lunar program was to determine the variation of antenna temperature as a function of phase angle for selected portions of the lunar surface. Observations must be restricted to those times when the atmospheric humidity is low and, in particular, when the radome material is dry. In order to complete one lunar month, several months of observing is necessary. The scope of the lunar observing program was therefore dictated by the availability of weather conditions suitable for observing and the time remaining for data reduction.

The experimental procedure was as follows. From knowledge of the angular size of the moon, the lunar center was located by means of scans in hour angle and declination. The antenna beam was then positioned west one lunar diameter so that the passage of the moon provided a scan from west to east across the sub-terrestrial point. Approximately, ten such "drift scans" were made on each day of observation as the moon crossed the meridian. A typical such drift scan made near first quarter is shown in Figure 1, along with a calibrating signal. The asymmetry in the scan, due to the temperature gradient across the lunar disk, is clearly seen.

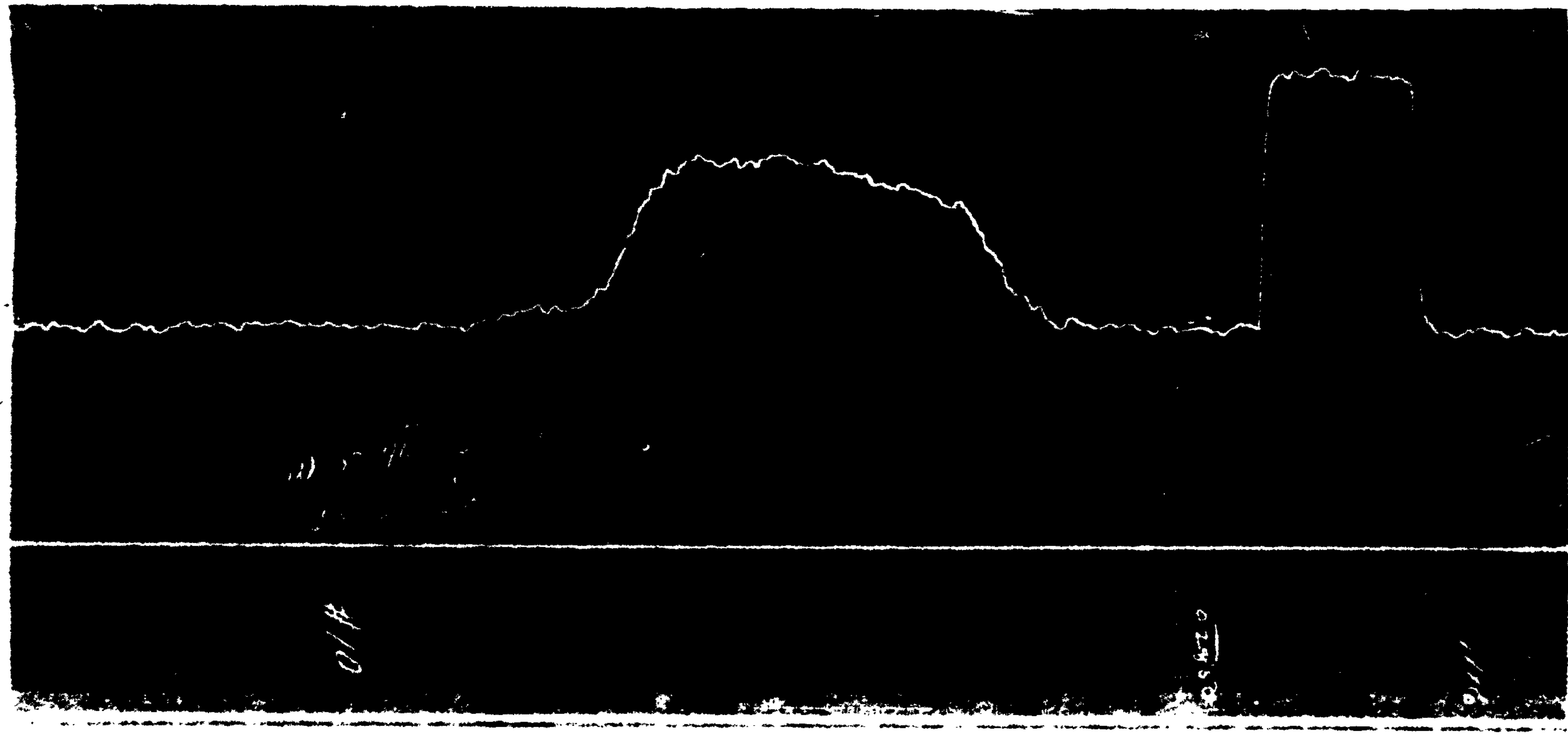

Figure 1

A Typical Drift Scan of the Moon, Near First Quarter. The Deflection on the Right is a Calibrating Signal.

From knowledge of the motion of the moon across the sky, the size of the lunar disk, and the chart speed of the recorder, a one to one correspondence between points on the drift scan and the position of the antenna boresight on the lunar disk can be made. Because of the finite size of the antenna beam, however, caution must be used when the edges of the lunar disk are approached.

Three points on the drift scans were chosen for consideration. They were the center and two points on each side of center, a distance corresponding to two antenna beamwidths. On the lunar disk, these points locate the antenna boresight at the center and half way between center and each edge along the equator. In terms of selenographic coordinates, the three areas of observation are centered at:

1. 0° latitude
   0° longitude
2. 0° latitude
   30° east longitude
3. 0° latitude
   30° west longitude

In terms of lunar formations, these three areas of observation are located in the regions:

1. Sinus Medii
2. South and east of Capernicus
3. Mare Tranquillitatus

The antenna beamwidth of 4 minutes of arc covers an area approximately 150 miles in radius on the lunar surface.

2.4 Observational Data

A total of fourteen (14) days of observation were obtained. The average daily antenna temperatures for each region of observation are shown in Table 1. The antenna temperatures have been corrected for atmospheric attenuation, but

TABLE 1

LUNAR OBSERVATIONAL DATA

Date	Antenna Temperature Degrees Kelvin Longitude		
	30° East	0°	30° West
Feb. 21	96	102	92
26	89	96	90
27	89	93	89
28	88	90	86
Mar. 7	93	110	112
15	116	129	111
22	80	89	82
25	84	91	84
26	85	89	84
28	84	90	79
29	83	90	88
Apr. 8	101	120	117
9	113	127	122
15	122	123	115

not for radome loss. Antenna temperature for the sub-terrestrial point can be converted to apparent brightness temperatures by multiplying by 1.7 to correct for radome loss and by 1.1 to correct for the estimated emissivity 0.9. An additional emissivity correction of 1.15 should be used for the other two areas.

The temperature data of Table 1 are shown as a function of date in Figure 2-4. The curves through the experimental points are not best fits in any mathematical sense, but are visual estimates intended only to indicate the cyclic behavior and show clearly the time span of 1-1/2 lunar months of observation.

2.5 Data Interpretation

Because of the ellipticity of the lunar orbit, the times between lunar quarters is not constant but depend upon time of perigee and apogee. Therefore, since the observation time extended over nearly two lunar months, the temperature data should be plotted as a function of the phase of the region under observation instead of time. This has been done and the resulting curves are shown in Figure 5-7. The points are the average of the temperatures for each day of observation and the bars show the standard deviation of the temperature measurements for that day. The fact that the scatter in the points is larger than the standard deviation is indicative of the pointing uncertainties.

Even a qualitative examination of the temperature behavior as a function of phase reveals some interesting phenomena.

The curves for the sub-terrestrial region and the region at 30° west longitude have approximately the same shape as those resulting from earlier work at the same wavelength, which were averages over the lunar disk. The temperature extremes lag full and new moon by approximately 40° phase angle. (See, for example, Reference 6). This phase lag is indicative of the low thermal conductivity of the lunar subsurface material. The temperature extremes for the 30° east longitude

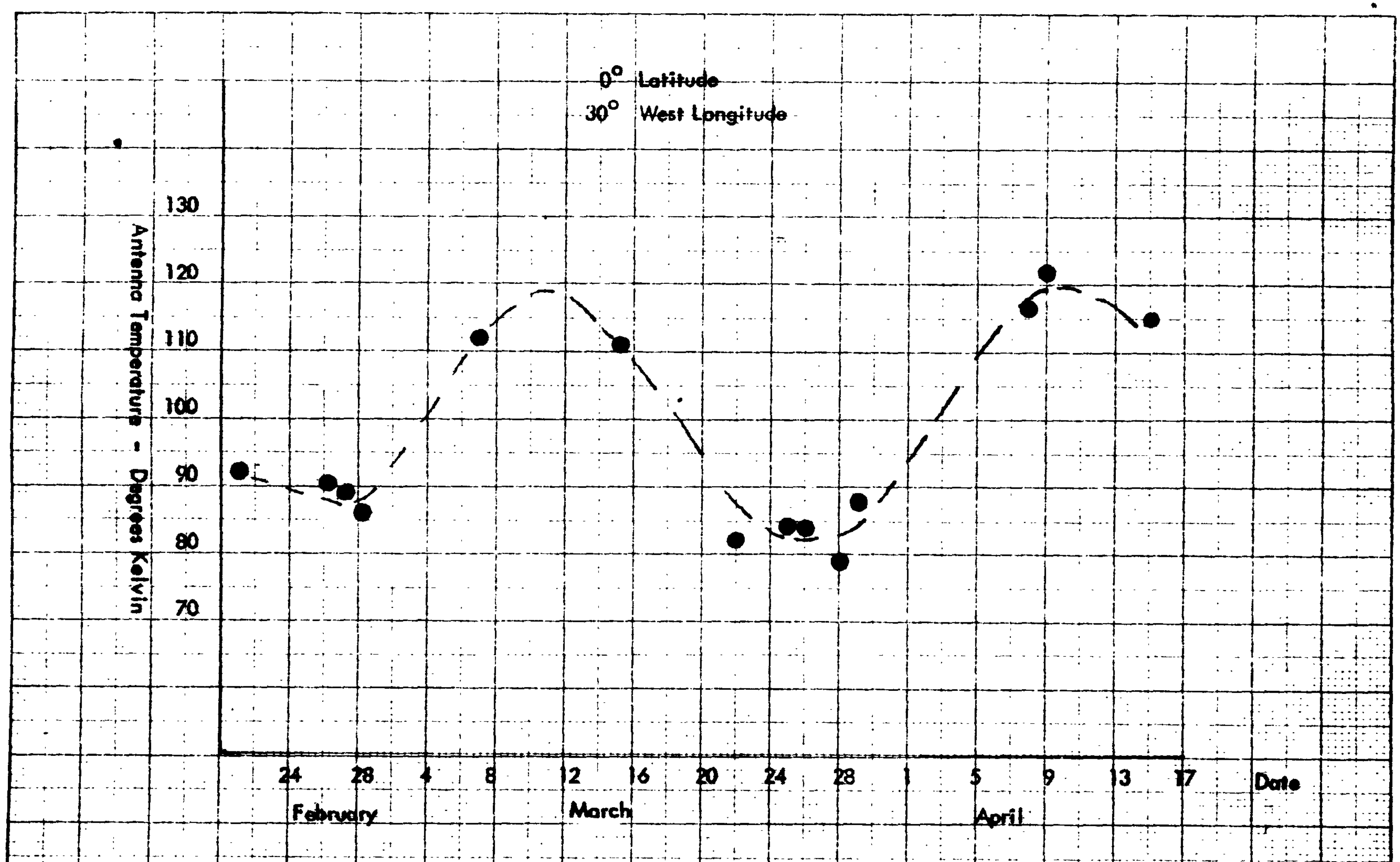

Figure 2

Antenna Temperature as a Function of Time for the Region at 30° West Longitude, 0° Latitude.

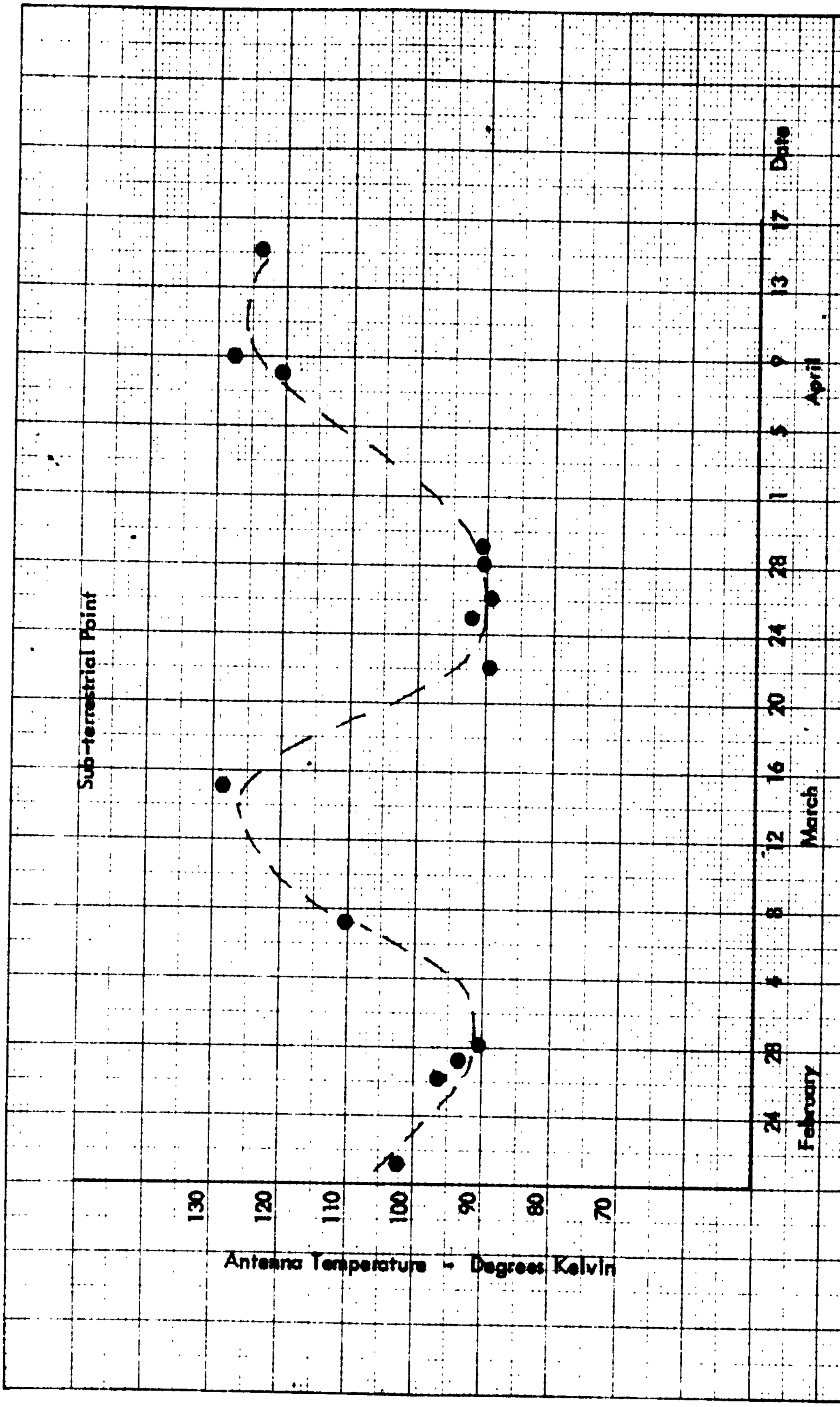

Figure 3

Antenna Temperature as a Function of Time for the Region at 0° Latitude, 0° Longitude.

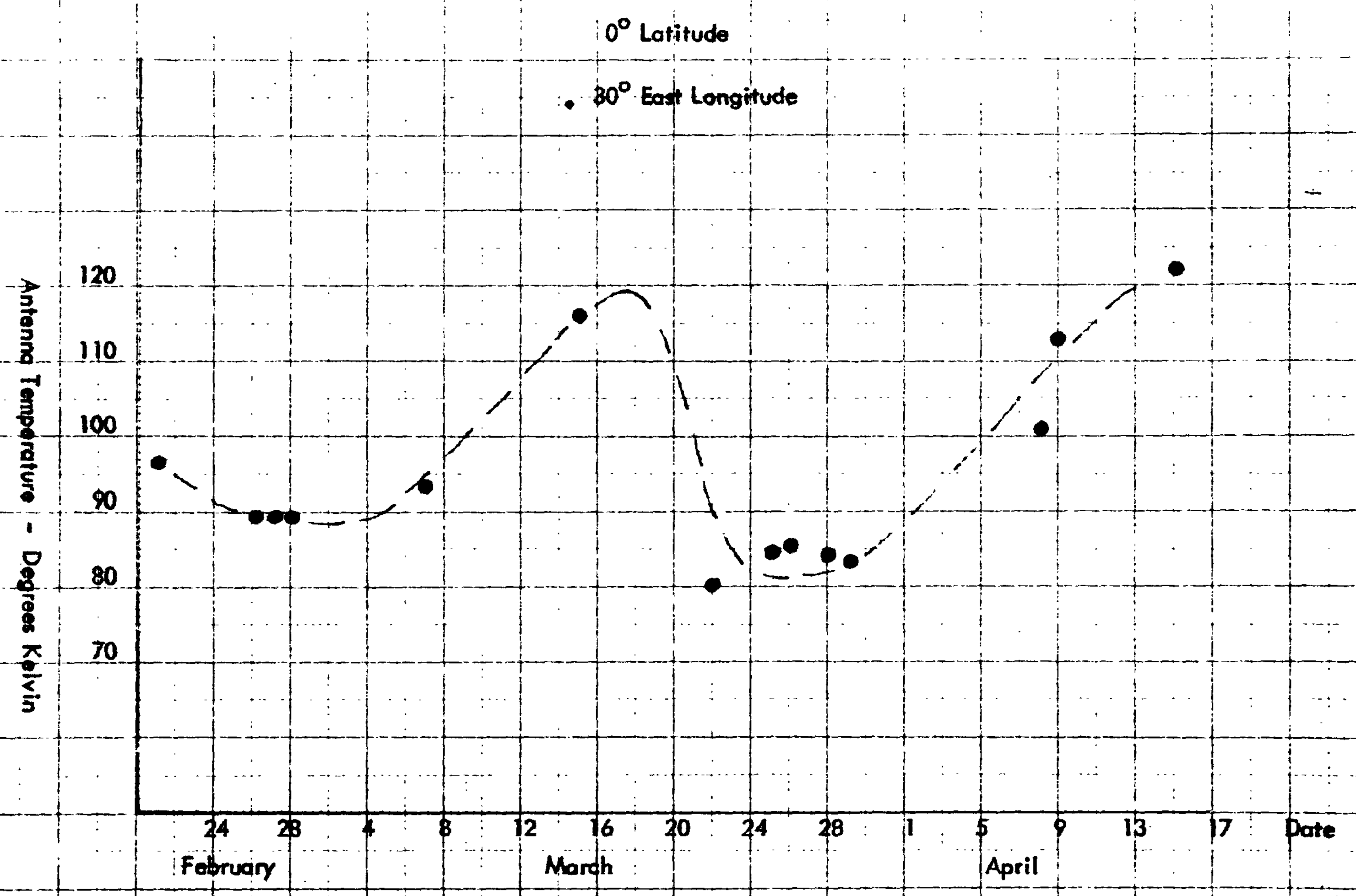

Figure 4

Antenna Temperature as a Function of Time for the Region at 0° Latitude, 30° East Longitude.

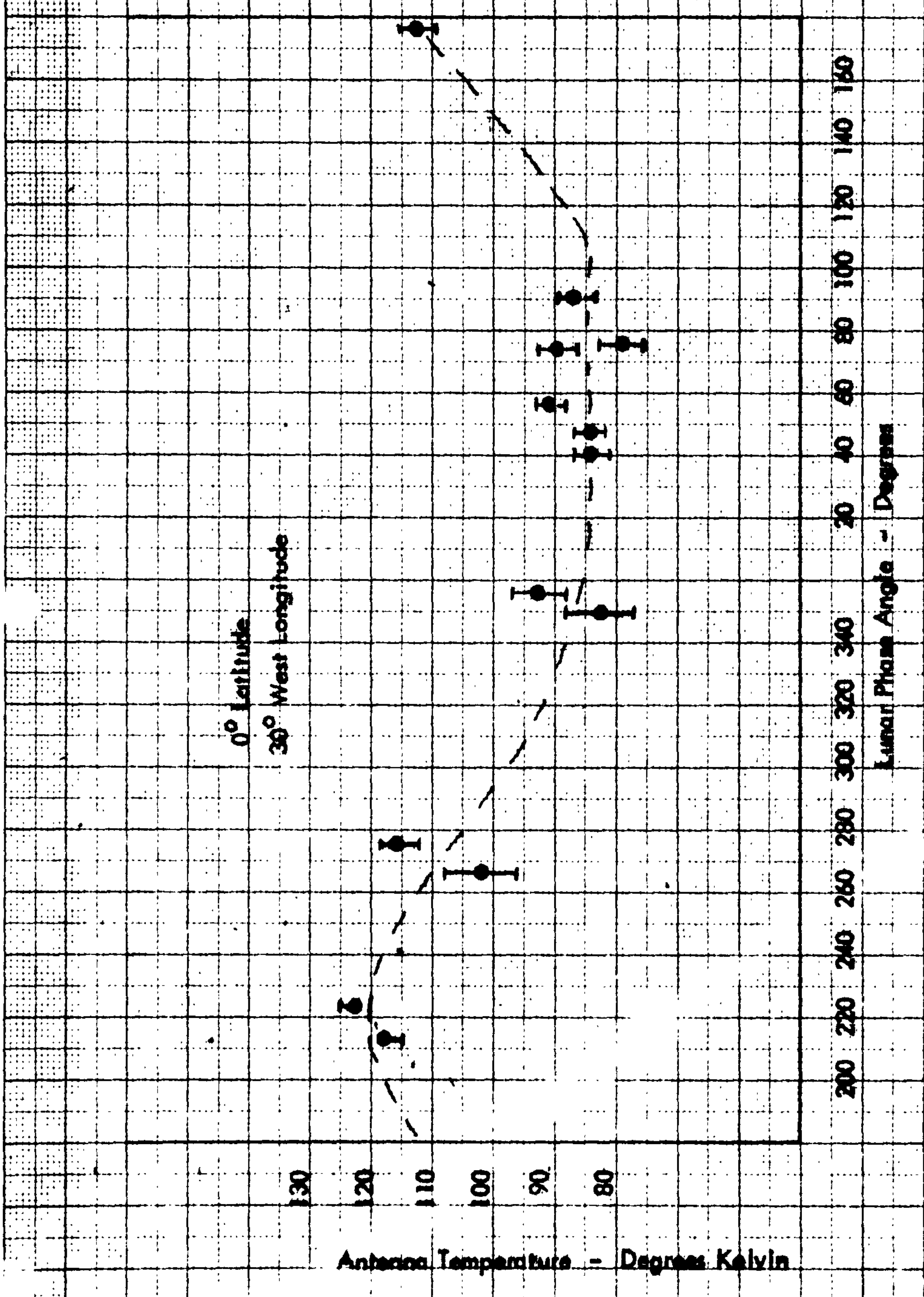

Figure 5

Antenna Temperature as a Function of Lunar Phase Angle for the Region at 0° Latitude, 30° West Longitude.

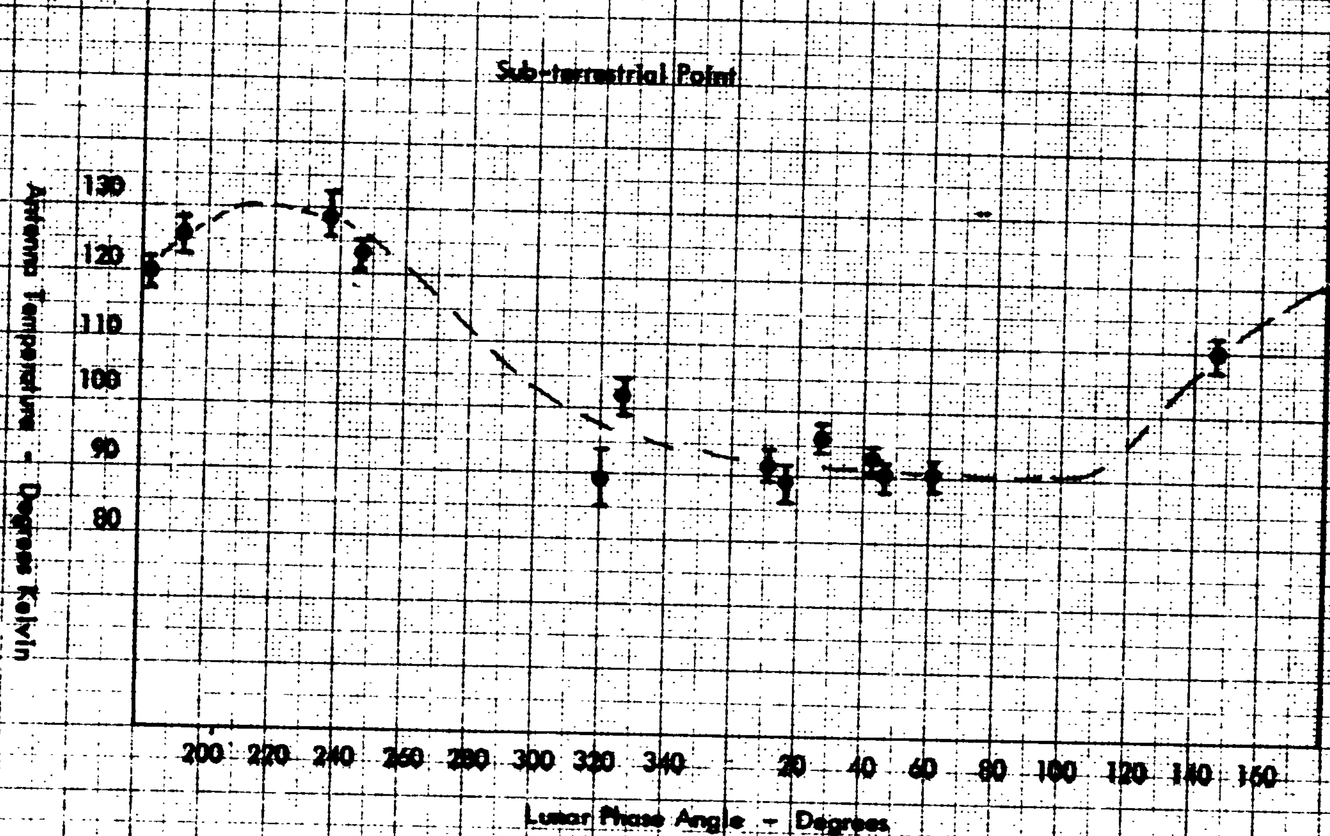

Figure 6

Antenna Temperature as a Function of Lunar Phase Angle for the Region at 0° Latitude, 0° Longitude.

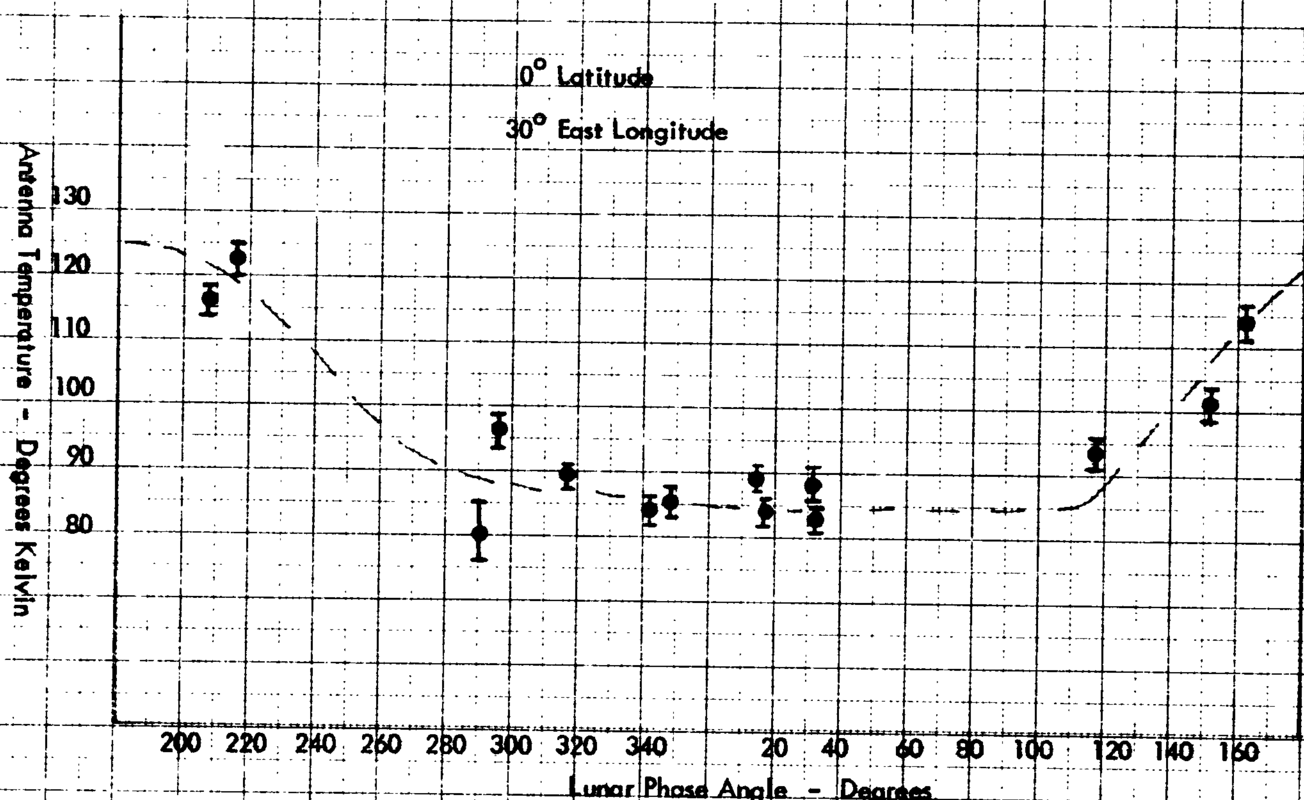

Figure 7

Antenna Temperature as a Function of Lunar Phase Angle for the Region at 0° Latitude, 30° East Longitude.

region, however, appear to coincide very nearly to new and full moon. This effect is particularly evident in Figure 7. A smaller phase lag, indicating a larger heating and cooling rate, could be explained by a higher value of subsurface thermal conductivity and/or a higher value of infrared surface emissivity.

In order to evaluate the data by the method outlined in the Appendix, the Fourier coefficients for the infrared surface temperature variations must be known. A theoretical curve developed by Tyler (Reference 6) which fits closely the experimental infrared temperatures versus phase is shown in Figure 8.

The infrared temperatures versus phase angle shown in Figure 8 was harmonically analyzed by an empirical method which gives the first six Fourier coefficients and their phase angles (Reference 11). The result of the harmonic analysis is shown in Table II . The values for the Fourier coefficients given here may be compared with those of Sinton (Reference 9) who reports 210°K, 157°K, 34°K, and 30°K, for the first four coefficients, with corresponding phase angles of -6°, 6°, and 159°.

The microwave temperature curves shown in Figure 5-7 were harmonically analyzed by the same method that was used for the infrared temperatures. The results are shown in Table III .

The temperature curves of Figures 5-7 are visual estimates based on only 14 experimental points. Quantitative interpretations of the Fourier coefficients and their phase angles in terms of the δ_n would be quite hazardous. In fact, the relative values of T_1' for the two regions East and West of the sub-terrestrial point are inconsistent with their corresponding phase angles. It is felt, therefore, that only qualitative interpretation of the data to date is justified. Based on the shape of the temperature versus phase curves, the conclusions that may be reached are as follows:

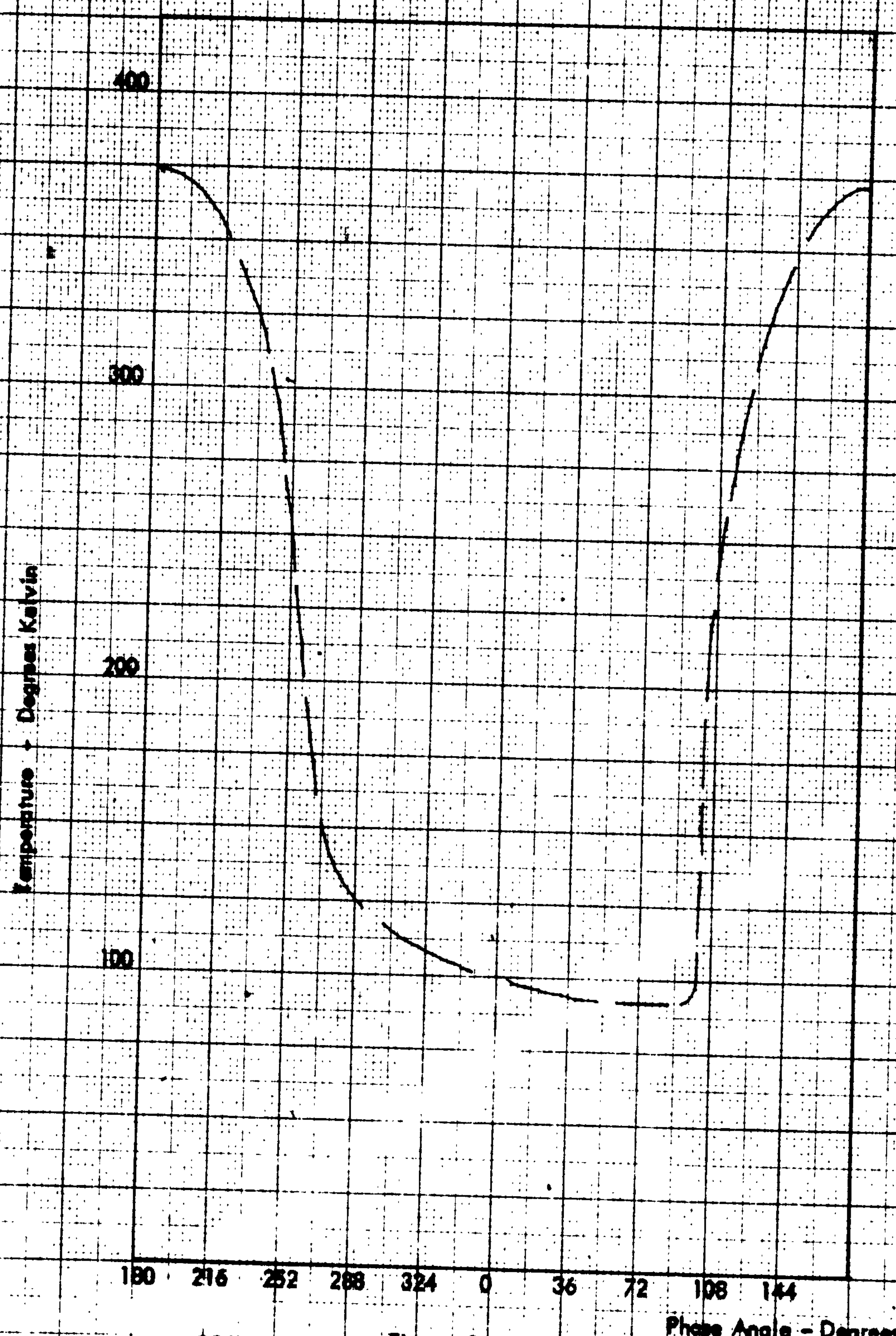

Figure 8

Infrared Temperature as a Function of Lunar Phase Angle.

TABLE II

FOURIER COEFFICIENTS
INFRARED TEMPERATURES

n	T_n °K	n Degrees
0	207	-
1	156	- 5
2	53	8
3	29	-21
4	27	10
5	16	71

TABLE III

FOURIER COEFFICIENTS
MICROWAVE TEMPERATURES
(λ = 8.5 mm)

n	T'_n	ϵ_n	T'_n	ϵ_n	T'_n	ϵ_n
	Degrees Kelvin	Degrees	Degrees Kelvin	Degrees	Degrees Kelvin	Degrees
	30° West	Longitude	Subterrestrial Point		30° East	Longitude
0	97	-	106	-	96	-
1	16	31	18	31	18	13
2	6	38	7	38	9	35
3	0.9	-21	1	-21	3	-8
4	0.6	10	0.7	10	1	-43
5	0.8	5	0.9	5	3	161

1. The region of Copernicus appears to be heating and cooling faster than the average lunar surface. This is evidenced by the general behavior of its subsurface temperature with time, and by the presence of relatively larger high harmonic content in the temperature curve.
2. The larger heating and cooling rate is consistent with a high subsurface thermal conductivity and/or a higher surface emissivity.

The above observations are in agreement with those of Murray and Wildey (Ref. 11), who report that the Copernicus region appears as a "hot spot" at 10 microns wavelength. Also, Lynn (Ref. 12-13) reports that the region near Copernicus exhibits a radar cross section at 8.5 mm wavelength that is 22% lower than five other areas at the same radial distance from the sub-terrestrial point.

There are two additional facts of interest that may be inferred from the data:

1. The average antenna temperatures for the two regions on each side of the sub-terrestrial point agree well, after correction by the secant of the observational angle, with the average antenna temperature of the sub-terrestrial point region. This fact indicates that the lunar surface does not radiate according to Lambert's Law at a wavelength of 8.5 mm.
2. The antenna temperatures for all three regions agree well, after correction for angle of observation, emissivity, and radome loss, with the average infrared temperature. This fact lends support to the lunar model chosen and the validity of the data.

The accumulation of further data will more accurately determine the variation of lunar temperature with phase and permit a better quantitative evaluation of the data.

3.0 VENUS OBSERVATIONAL PROGRAM

3.1 Background

Over the past years, considerable new information about the planet Venus has come from microwave observations. The earliest of these was pioneered at the Naval Research Laboratory by C. H. Mayer and his associates. More recently, accelerated activity of scientists of the Soviet Union in radiometric measurements has been noted, the results of which are contained in this section.

The status of microwave observations of Venus as of the beginning of the program described here is illustrated in Table IV.

The data shown in Table IV is plotted in Figure 9. The significant feature of the spectrum is the substantial difference between the infrared temperature of about 250°K (Ref. 26-27) and the long wavelength radiometric temperatures.

Spectroscopic evidence exists for the presence of carbon dioxide, nitrogen, and water vapor above the cloud cover of Venus. The temperature, as a function of wavelength, and the possible composition of the atmosphere, combine to yield the following concept of the physical environment.

The measurements at 3 and 10 cm offer substantial evidence for purely thermal radiation, originating from the surface of the planet itself. Correspondingly, there is little doubt that the infrared radiation originates in the upper layers of the atmosphere of Venus. It appears therefore that the temperature of the planet changes from 600°K at the surface to about 300°K in the upper layers of the planet's atmosphere.

It is significant to note from Figure 8 that millimeter wavelengths apparently lie in a transition region between the infrared and the centimeter wavelength observations. Measurements at 8.5 mm wavelength are therefore of great interest since this region is most sensitive to the interpretation of the various models of the atmosphere

TABLE IV

RADIO OBSERVATIONS OF VENUS

λ (cm)	Freq. Mc/s	T_B °K	Date of Observation	Reference
21	1420	600 ± 200	April, 1961	15. Lilley
12.5	2388	600 ± 200	April 21 - May 8, 1961	16. Stelzried and Schuster
10.2	2940	600 ± 65	Sept. 17 - Oct. 10, 1959	17. Mayer et al
10.0	3000	622 ± 50	March 15 - August 2, 1961	18. Drake
9.4	3200	580 ± 160	June 25, July 27, 1956	19. Mayer et al
3.75	8000	585 ± 7*	July 7 - Oct. 4, 1959	20. Drake
3.4	8800	575 ± 60	Feb. 12 - Mar. 5, 1958	17. Mayer et al
3.37	8900	575 ± 58	April 18, 19, 1958	21. Alsop et al
3.15	9500	595 ± 55	May 5 - June 23, 1956	19. Mayer et al
0.86	35000	410 ± 160	Jan. 29, Feb. 5, 6, 11, 1958	22. Gibson et al
0.80	37500	315 ± 70	Sept. 18, 1959	23. Kuzmin et al
0.43	70000	350 ± 50*	April, 1961	24. Grant
0.40	75000	390 ± 120	April, 1961	30. Kuzmin et al

* The error quoted does not include any allowance for error in antenna calibration.

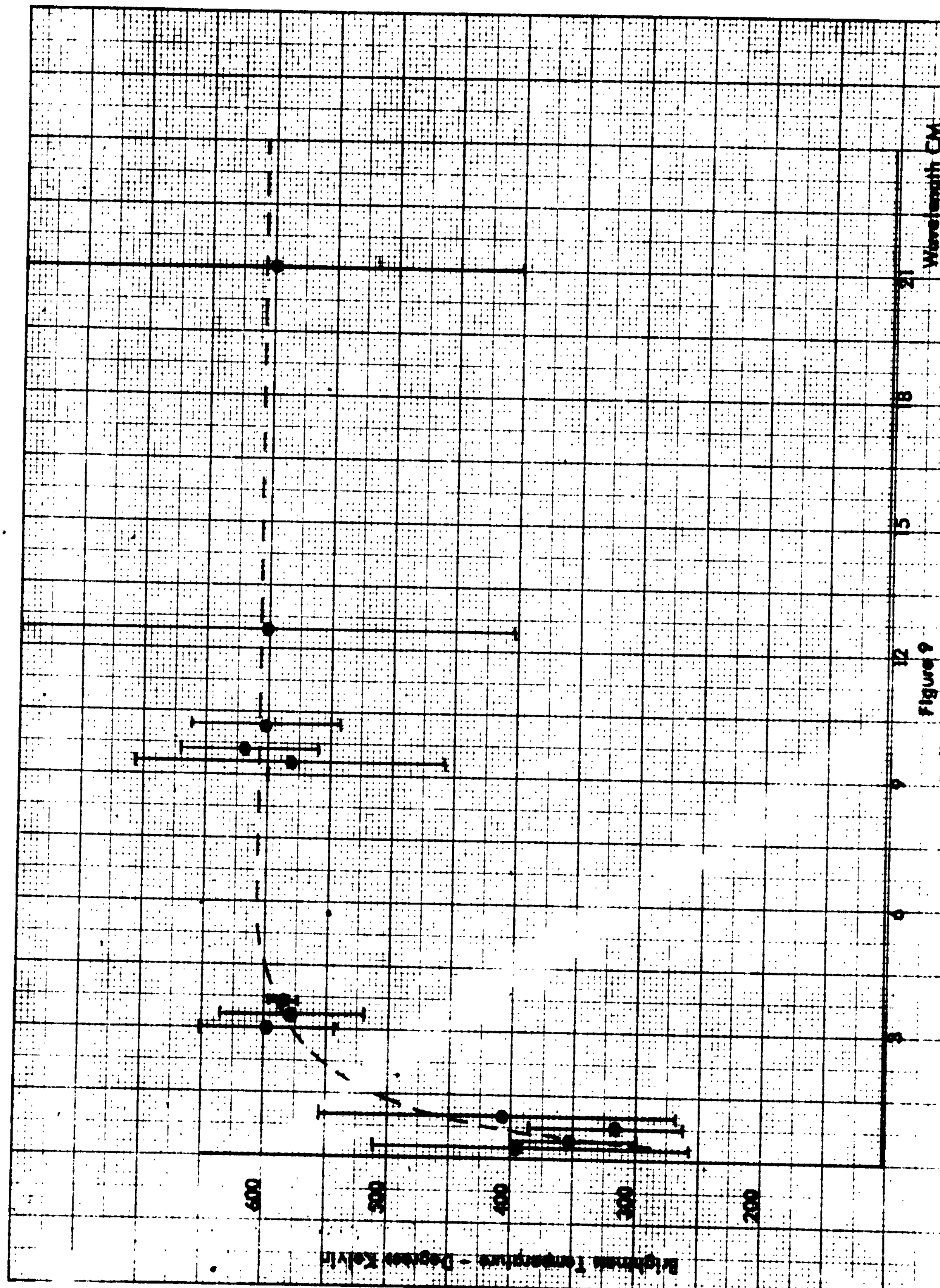

Figure 9
Radio Spectrum of Venus

(Ref. 29).

An additional interesting effect has been noted in radio observations. There is an apparent systematic change in radio brightness temperature with optical phase of the planet. This effect has been observed at 3 cm (Ref. 19), 10 cm (Ref. 18), 8 mm (Ref. 23), and 4 mm (Ref. 30). The 3 cm and 10 cm results are consistent with a slow rotation rate, and the fact that the long wavelength radio radiation has its origin at the surface of the planet. The millimeter "phase effect" is difficult to understand, however, since the bulk of the radiation at this wavelength should originate from the atmosphere of the planet which does not exhibit any annual temperature variation (Ref. 26, 27).

Further observations of the planet Venus, particularly at millimeter wavelengths, are most important for a better determination of the brightness temperature and further verification of a change in brightness temperature with optical phase.

3.2 The Experimental Procedure

The objective of the experimental part of the Venus program was to observe the planet 8.5 mm for as long as possible near conjunction in order to determine the brightness temperature and its change, if any, with phase.

The planet Venus was first observed on November 7, 1962. At the time of observation, Venus was nearly on the horizon and covered by clouds from an approaching rainstorm; the signal-to-noise ratio was, therefore, poor and no quantitative data was taken. It was determined, however, that the radio boresight of the antenna was displaced in declination by 44 minutes of arc (11 beamwidths). Errors in pointing were expected from the results of previous tests on the antenna.

After four days of inclement weather, during which time tests and adjustments were made to optimize equipment performance, the observing program was begun on November 12, 1962. In the interest of minimizing indeterminate measurement uncertainties, observations were restricted to days which were clear and, in particular, when the radome material was dry. Furthermore, each daily observational period was near meridional crossing, when the planet's elevation angle was maximum, in order to further reduce atmospheric attenuation effects.

The experimental procedure was as follows:

1. The planet was located radiometrically.
2. While tracking in hour angle, the antenna was moved slowly in hour angle and declination so as to center the planet in the antenna beam.
3. The antenna beam was then positioned a few minutes west of the planet, which then drifted through the beam at sidereal rate.
4. After the planet had moved completely through the beam, the noise tube was energized, thereby providing a $5^{\circ}K$ calibrate signal after each drift curve.*
5. The antenna beam was repositioned when the declination of Venus changed by one-half beamwidth (2 minutes of arc) as indicated by the ephemerides.
6. After conjunction, as Venus was rapidly receding from the earth, it was necessary to superimpose a small scan rate in hour angle, increasing the time of passage through the beam, thereby permitting the use of larger time constants to improve the signal-to-noise ratio.

Two drift curves, obtained on November 28, 1962 and December 9, 1962, are shown in Figure 10 and Figure 11. These curves are typical and indicate the

* Except on the first day, when a $160^{\circ}K$ calibrate signal was used, with the appropriate change in sensitivity afterwards.

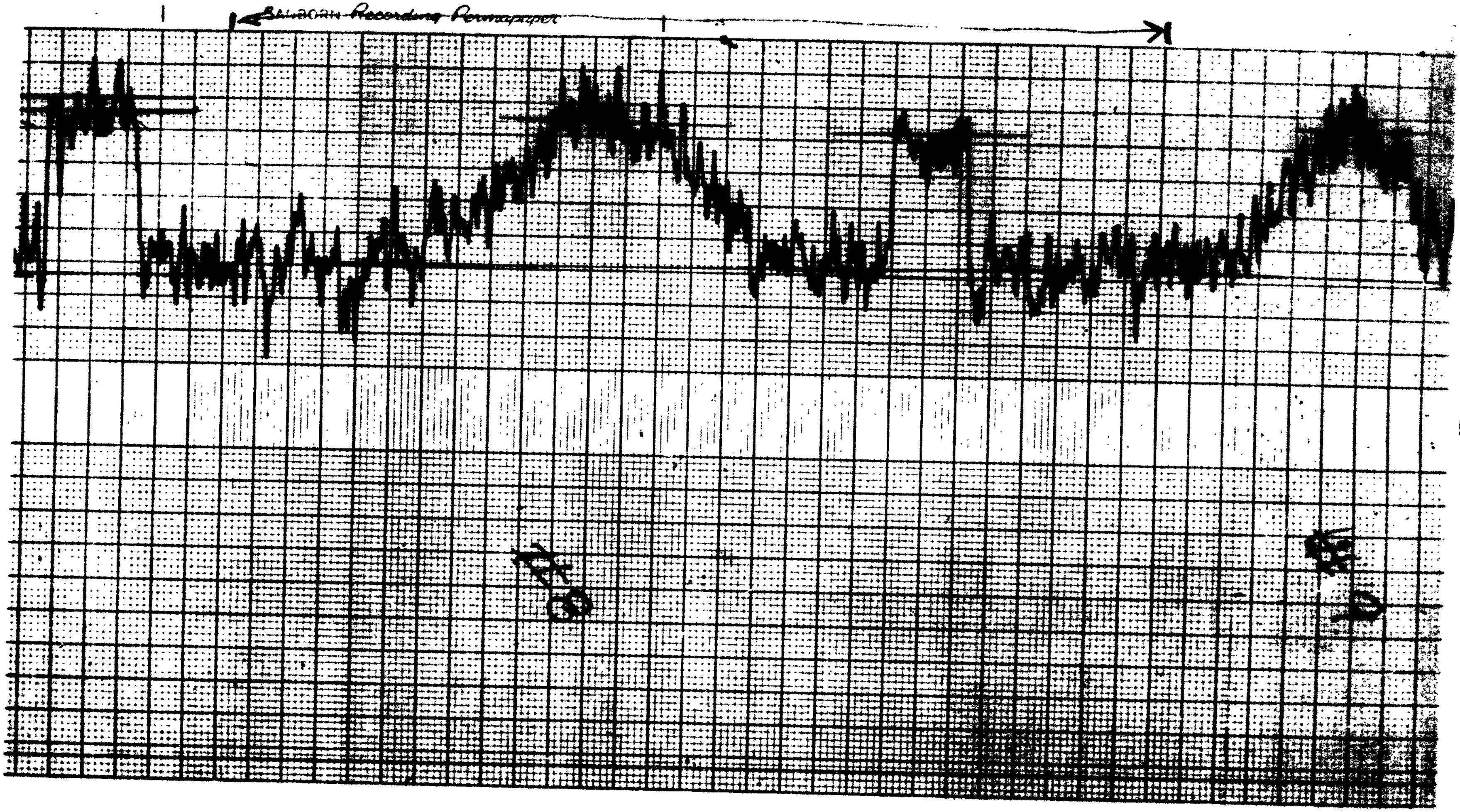

Figure 10

Venus Drift Curves - November 28, 1962

(Drift Rate - Sidereal; Chart Speed - 1 mm/second; Time Constant 1.5 seconds; and Calibration Deflections - 5°K)

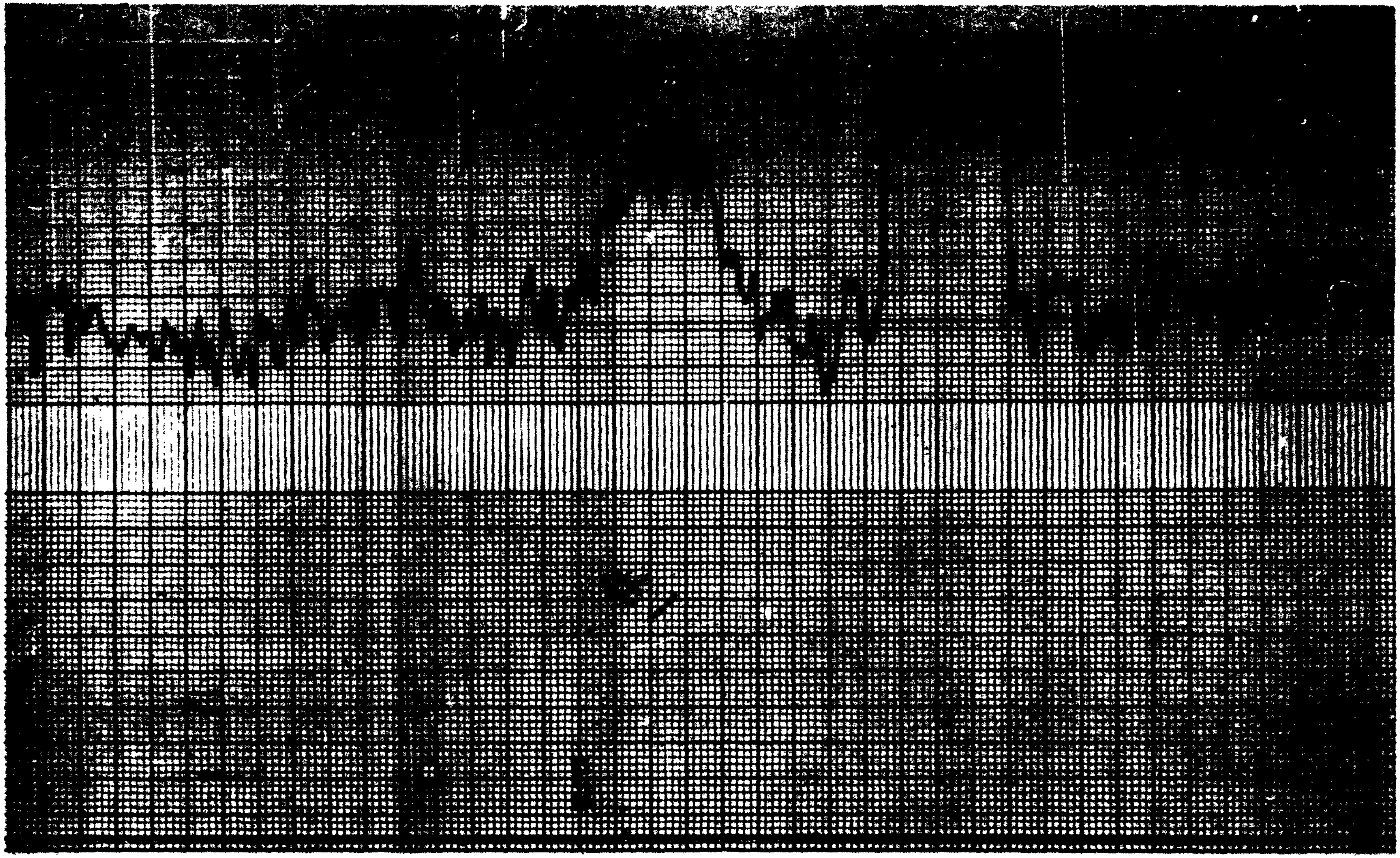

Figure 11

Venus Drift Curve - December 1962

(Drift Rate - Approximately one-half Sidereal; Chart Speed - .1 mm/second; Time Constant - 8 seconds; and Calibration Deflection - 5°K) nature of the raw radiometric data.

3.3 Data Reduction and Interpretation

For a period of four weeks following conjunction, a total of seven days of observation at 8.5 mm were accumulated before the signal from Venus became obscured by noise. During this time, the antenna temperature, due to the planet, decreased from about 7°K to about 3.5°K. The measured antenna temperatures as a function of time are shown in Figure 12.

The antenna temperatures were converted to black body brightness temperatures as follows:

$$T_B = \frac{\lambda^2 L}{\eta \, \Omega \, A} \quad T_A$$

where:

T_A = antenna temperature, corrected for atmospheric attenuation

T_B = brightness temperature

λ = wavelength

Ω = solid angle subtended by Venus

A = antenna aperture area

L = radome loss

η = antenna efficiency

The resulting brightness temperatures are shown in Figure 13.

The solid angle employed in the calculation was assumed to be that of the optical disk of the planet as tabulated in the ephemerides.

The radiometer was calibrated by means of a standard 10,000°K noise tube, the signal from which was reduced to 5°K by means of a directional coupler and an attenuator.

Two particular problems which beam upon the absolute accuracy of the

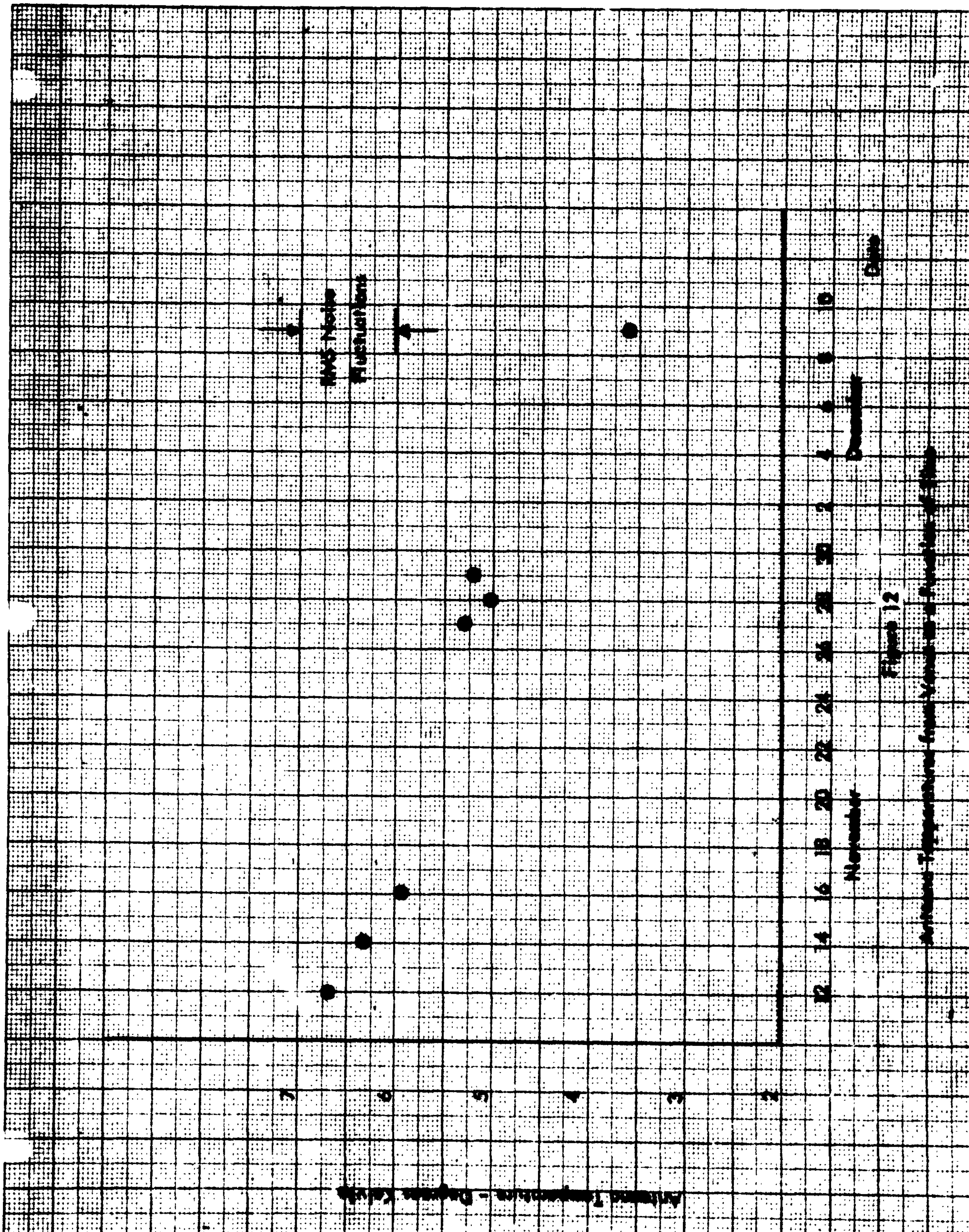
RMS Noise Fluctuations
Antenna Temperature - Degrees Kelvin
7
6
5
4
3
2
12
14
16
18
20
22
24
26
28
30
2
4
6
8
10
November
December
Date

Figure 12

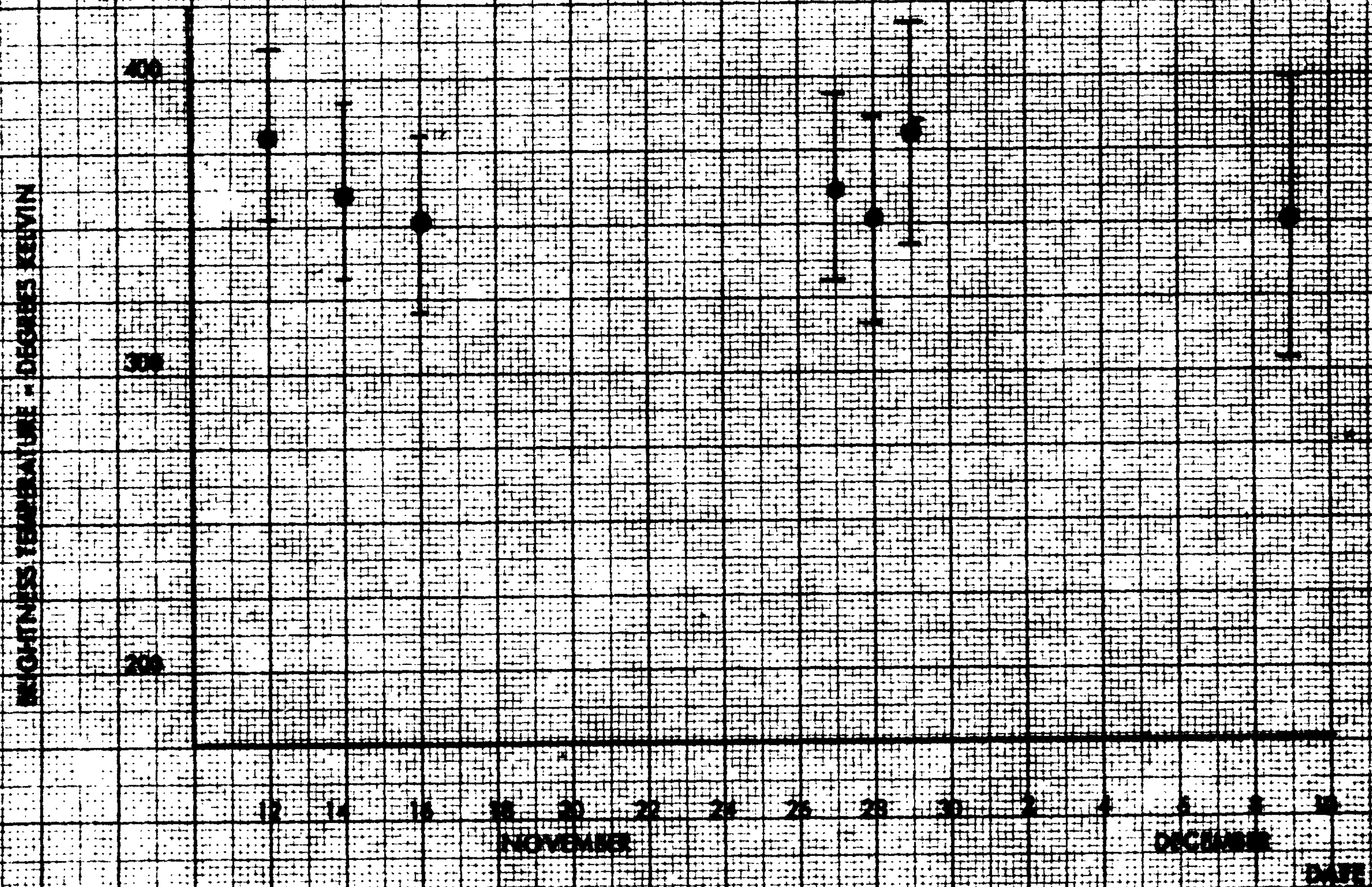

Figure 13 VENUS BRIGHTNESS TEMPERATURES AS A FUNCTION OF TIME. THE BARS SHOW THE RMS NOISE FLUCTUATIONS IN TERMS OF EQUIVALENT UNCERTAINTY IN BRIGHTNESS TEMPERATURE.

results are the antenna efficiency η , and, since these observations were carried out from within a radome, the problem of the radome loss. The antenna efficiency, combined with the radome loss, was measured directly by observing a known source located eight miles from the antenna. (The antenna was refocused at infinity when observing Venus.) The combination of true antenna efficiency and radome loss, η/L, were treated as an effective antenna efficiency. The value resulting from the measurements was $\eta/L = 30\%$. This value has been adopted in calculating the brightness temperature.

In the wavelength region of these observations, the attenuation of the earth's atmosphere, although small, is not entirely negligible. A value of zenith attenuation of 0.2 decibels was adopted in the data reduction procedure. In addition to the usual corrections for zenith angle of observation, a small additional correction for each observation was included for dependence upon relative humidity. The relative humidity was monitored throughout the observations.

Based on the observational and reduction procedures given above, a summary of the resulting brightness temperatures is given in Table V. The mean brightness temperature, weighted according to the signal-to-noise ratio on each day of observation, is $360^{\circ}K \pm 100^{\circ}K$. The uncertainty quoted is an estimate of the total uncertainty of the absolute values; it is therefore the estimated limit of error. It includes an estimate of the combined antenna-radome loss uncertainty, the achieved signal-to-noise ratio, the pointing inaccuracies of the antenna, calibration uncertainty, and a contribution due to atmospheric attenuation. These individual contributions have been listed in order of their estimated magnitude, the antenna efficiency-radome loss combination being the more serious error source. The value reported here of $360^{\circ}K \pm 100^{\circ}K$ may be compared with that given by Kuzmin and Solomonovich (Ref. 31) of $374^{\circ}K \pm 75^{\circ}K$.

TABLE V

VENUS OBSERVATIONAL DATA

Date	Number of Drift Curves	Mean Antenna Temperature (°K)	Mean Brightness Temperature (°K)	k
November 12	15	6.75	383	0.003
November 14	9	6.22	355	0.004
November 16	9	5.83	346	0.006
November 27	4	5.26	357	0.066
November 28	7	5.02	352	0.072
November 29	3	5.14	376	0.082
December 9	3	3.59	349	0.172

The uncertainties in the relative values of brightness temperatures are felt to be much better known than the absolute values. Because of the experimental procedure, the primary source of relative error should be the uncertainties in data readout from the poor signal-to-noise ratio; the rms signal-to-noise ratio should, therefore, be indicative of the probable rms error in the relative temperatures.

The observational data covered a range of phase angle from 174° on November 12 to 130° on December 9. This corresponds to a range in the fractional illuminated disk, k, from .003 to .172. Although the range in phase angle is limited, the dependence of brightness temperature on k may be compared with the earlier results recorded by Kuzmin and Salomonovich. The Soviet 8 mm data suggests a rather strong dependence of the 8 mm brightness temperature with phase angle. In addition, the same effect has been reported at a wavelength of 4 mm by Kizlyakov, Kuzmin, and Salomonovich (Ref. 30). The quality of all data obtained so far warrants only the use of a highly simplified model. Only the dependence of the resultant brightness temperature by date upon the corresponding value of k has been investigated. Following this assumption, a test for a crude indication of the temperature difference on the light and dark sides of the planet is as follows. If T_1 and T_2 are the temperatures of the light and dark sides respectively, and k is the fraction of the planetary disk illuminated by the sun, then the observed brightness temperature T_B is given by:

$$T_B = k\ T_1 + (1 - k)\ T_2 = T_2 + (T_1 - T_2)\ k$$

Therefore, a plot of T_B versus k should yield a straight line whose slope is $(T_1 - T_2)$ and whose intercept is T_2.

The brightness temperatures versus k, were "best fitted" by the least squares procedure to a straight line. During the first day of observation, some question of the constancy of the calibration signal arose. The first data point, since its validity was questionable, was omitted from the least squares procedure. The best fit was:

$$T_B = 350 + 50\,k$$

The brightness temperature versus k is shown in Figure 14. The bars on the data points show the rms noise fluctuations converted to equivalent uncertainty in brightness temperature.

A difference in temperature between the sunlit and dark sides of Venus is not clearly evident in the results reported here; it is estimated that a sunlit to dark side temperature differential of 200°K would have been detected. The slope of the Soviet curve at 8.5 mm is 375 (Ref. 31).

From the preliminary results given here, although the quantity of data is limited, there is no substantial difference in temperature between the sunlit and dark sides of the planet Venus at 8 mm wavelength. This result is in agreement with the recent preliminary results of the Mariner R microwave radiometer experiment (Barath, et al., 1963).

The contents of this section have been submitted to the *Astrophysical Journal* for publication.

A further more extensive publication will be made after further data analysis and error investigations have been made. Such publications will be submitted to NASA for prior approval.

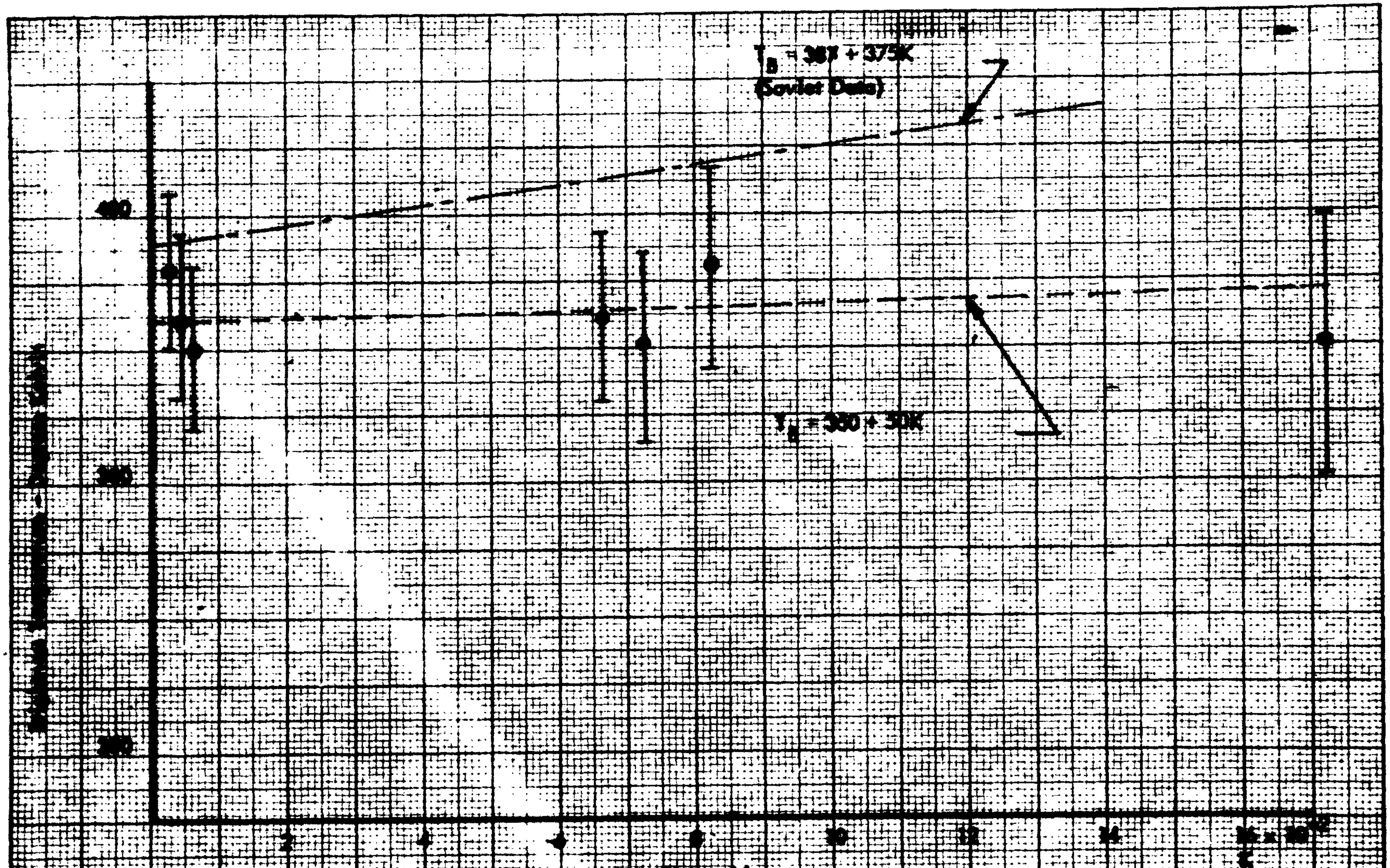

Figure 14
Mean Brightness Temperature as a Function of the Fraction, K, of the Planetary Disk Illuminated by the Sun

REFERENCES

1. Wesselink, A.J., "Heat Conductivity and the Nature of the Lunar Surface Material", Bulletin of the Astronomical Institute of the Netherlands, Vol. 10, 1948, pp. 351-363.
2. Piddington, J.H.,and Minnett, H.C., Australian Journal of Scientific Res., Vol. 2, 1949, pp. 63-77.
3. Salomonovich, A.E., "Radio Emission of the Moon at 8 mm", Astron. Journal Acad. Sciences, U.S.S.R., Translation Published by Amer. Inst. Physics, A.J., Vol. 2, 1955, pp. 112-118.
4. Jaeger, J.C., "Conduction of Heat in a Solid with Periodic Boundary Conditions with an Application to the Surface Temperature of the Moon", Proc. Camb. Phil. Soc., Vol. 49, 1953, pp. 355-359.
5. Jaeger, J.C., "The Surface Temperature of the Moon", Australian Jour. of Phys., Vol. 6, 1953, pp. 10-21.
6. Tyler, W.C., "The Experimental Measurement and Theoretical Interpretation of Thermal Radiation from the Lunar Surface", Report TN2H4N, Research Laboratory, USAOMC, Redstone Arsenal, Alabama.
7. Lettau, H., "On the Heat Budget of the Moon and the Surface Temperature Variations During an Eclipse, Geofisica Pura e Applicata, Vol. 19, 1951, pp. 1-18.
8. Muncy, R.W., "Calculations of Lunar Temperatures", Nature, Vol. 181, 1958, pp. 1458-1459.
9. Sinton, W.H., "Temperatures on the Lunar Surface", Physics and Astronomy of the Moon, ed. Kopal, Z., p. 146, Academic Press, New York, N.Y. (1962)

10. Kaidanovskii, N.L., "Study of the Moon by Means of Radio", The Moon, A Russian View, ed. Markov, A.V., pp. 223-245, University of Chicago Press, Chicago, Ill. (1962).

11. Scarborough, J.B., Numerical Analysis, pp. 558-568, The John Hopkins Press, Baltimore, Md. (1962).

12. Murray, B.C., and Wildey, R.L., "Stellar and Planetary Observations at 10 Microns", Astrophy. J., Vol. 137, No. 2, p. 692, 1963.

13. Lynn, V.L., "8.6 Millimeter Radar Reflections from the Moon", paper presented at 44th Annual Meeting of the American Geophysical Union, 1963, April 17-20, Washington, D.C.

14. Lynn, V.L., private communication.

15. Lilley, A.E., "The Temperature of Venus", Astrophy. J., Vol. 66, p. 290.

16. Stelzried, C.T., and Schuster, D., Jet Propulsion Laboratory Technical Report No. 32-132, ed. W.K. Victor, R. Stevens, and S.W. Golomb, pp. 74-76, Pasadena, Calif., August 1, 1961.

17. Mayer, C.H., McCullough, T.P., and Sloanaker, R.M., paper presented to the XIII General Assembly, URSI, London, September 5-15, 1960.

18. Drake, F.D., Publ. Nat. Rad. Astr. Obs., Vol. 1, No. 11, p. 165, 1962.

19. Mayer, C.H., McCullough, T.P., and Sloanaker, R.M., Proc. I.R.E., 46, 260, 1958.

20. Drake, F.D., quoted by C.H. Mayer in "Planets and Satellites", Vol. III of The Solar System, ed. G.P. Kuiper and B.M. Middlehurst, Chapter 12, University of Chicago Press, Chicago, Illinois, 1961.

21. Alsop, L.E., Giordmaine, J.A., Mayer, C.H., and Townes, C.H., Astrophy. J., 63, 301 (1959).

22. Gibson, J.E., and McEwan, R.J., Proc. IAU Symp. No. 9, URSI Symp. No. 1, ed. R.N. Bracewell, pp. 50-52, Stanford University Press, Stanford, Calif.

23. Kuzmin, A.D. and Salomonovich, A.E., Astron. J. (U.S.S.R.) Vol. 37, pp. 297-300, 1960.

24. Grant, C.R., paper presented at A.A.S. meeting, Denver, Colorado, December, 1961.

25. Kislyakov, A.G., Kuzmin, A.D., and Salomonovich, A.E., Radiofizika, Vol. 4, p. 573, 1961.

26. Pettit, E., and Nicholson, S.B., Pub. Astron. Soc. of Pacific, Vol. 67, p. 293, 1955.

27. Sinton, W.M., and Strong, J., Astrophys. J., Vol. 131, p. 470, 1960.

28. Chamberlain, J.W., and Kuiper, G.P., Astrophy. J., Vol. 124, p. 399, 1956.

29. Barrett, A.H., J. Geophy. Research, Vol. 65, p. 1835, 1960.

30. Kislyakov, A.G., Kuzmin, A.D., and Salomonovich, A.E., "4-mm Radio Emission from Venus", Soviet Astronomy-AJ, Vol. 6, No. 3, pp. 328-332, 1962.

31. Kuzmin, A.D., and Salomonovich, A.E., "Observations of Radio Emission from Venus and Jupiter at 8 mm Wavelength", Soviet Astronomy-AJ, Vol. 6, No. 4, pp. 518-524, 1963.